The Report Committee for Weiwei Wang
Certifies that this is the approved version of the following report:

Study of Natural and Hydraulic Fracture Interaction Using Semi-Circular Bending Experiments

APPROVED BY
SUPERVISING COMMITTEE:

Supervisor: _____
Jon E. Olson

Co-Supervisor: _____
Maša Prodanović

Study of Natural and Hydraulic Fracture Interaction Using Semi-Circular Bending Experiments

by

Weiwei Wang, B.E.; B.S. Petroleum ENGR.

Report

Presented to the Faculty of the Graduate School of

The University of Texas at Austin

in Partial Fulfillment

of the Requirements

for the Degree of

Master of Science in Engineering

The University of Texas at Austin

May 2014

Dedication

To my devoted parents for their endless love and support

Acknowledgements

I would like to express my deepest gratitude to my advisors Dr. Jon E. Olson and Dr. Maša Prodanović for their consistent support, patience and guidance throughout the years. I thank Shell-UT Unconventional Research (SUTUR) for the project funding. I thank Dr. Jon Holder, Ben Bahorich and Gary Miscoe for their help in lab, thank Dori Coy and Frankie Hart for their administration and registration help, and thank Roger Terzian and John Cassibry for providing computer supports.

I am grateful to my colleagues from Dr. Olson and Dr. Prodanović's research group for their friendship, advice and suggestions, especially to Kan Wu, Kaimin Yue, Valerie Gono, Hunjoo Lee, Kashif Naseem and Adenike Tokan-Lawal. I would also like to thank my good friends who offered much needed companionship as we completed the program. Finally, I sincerely thank my parents for their endless support and love.

Abstract

Study of Natural and Hydraulic Fracture Interaction Using Semi-Circular Bending Experiments

Weiwei Wang, M.S.E

The University of Texas at Austin, 2014

Supervisor: Jon E. Olson

Co-Supervisor: Maša Prodanović

Hydraulic fracturing is an indispensable technique for developing unconventional resources such as shale gas and tight oil. When hydraulic fractures interact with pre-existing natural fractures, it can result in a complex fracture network. The interaction depends on in-situ stresses, rock and natural fracture mechanical properties, approach angle and hydraulic fracture treatment parameters.

Most simulation studies treat natural fractures as frictional interfaces with cohesive properties. However, from core observation, partially cemented and fully cemented natural fractures are widely present and it is not clear whether they would fit the common description. In this study, semi-circular bending test is utilized to examine the propagation paths and strength of samples with pre-existing cemented fractures. Synthetic hydrostone samples are used to represent the rock and different inclusion slices with different

mechanical properties are used to mimic cemented natural fractures. In a series of experiments, we assess the influence of the fracture approach angle, inclusion strength, and inclusion thickness on fracture propagation.

Current results show that fractures tend to cross the inclusion when the approach angle is high and divert into the inclusion when the approach angle is low. The crossing surface is not a clean cut, but often has a jog distance. The thickness of the inclusion does not change the crossing/diverting behavior for orthogonal approaching samples, however it does change the jog distance along the interface. Preliminary simulation results using finite element software, ABAQUS, are presented better to analyze the experimental observations. The assessments of fracture interaction in this study are in good agreement with previous work and theories.

Table of Contents

List of Tables

List of Figures

CHAPTER 1: Introduction

1.1 Motivation

Hydraulic fracturing is the fast developing technology facilitating the success of many major unconventional plays in the US. It has been used to stimulate up to 70% of the gas wells and 50% of the oil wells in the North America (Renard et al. 2008). Proper understanding of the fracturing process is important to maximize fracture conductivity, improve hydrocarbon production and reduce completion investment. Micro-seismic data shows that many unconventional formations are naturally fractured. The pre-existing natural fractures can be reactivated during hydraulic fracture treatment, resulting in complicated fracture networks (Fisher et al. 2002; Maxwell et al. 2002; Le Calvez et al 2007). The fracture network can be problematic. For example, if the natural fractures are connected to a water zone, the hydraulic fractures connected to them would provide bad well stimulation result. Further, the open natural fractures can also capture treatment fluids and prevent new fractures from forming (Gale et al. 2007). Therefore, modeling hydraulic fracture propagates interacts with a natural fracture (that may be open, partially open, or completely sealed) in shale formation is a research topic of interest, which integrates multiple disciplines, such as rock physics, solid mechanics, and reservoir geomechanics.

In order to improve the accuracy of complex hydraulic fracture network modeling, a full analysis of natural and hydraulic fracture interaction is required. Fundamentally, if the frictional resistance or cohesion of a natural fracture is sufficient to prevent slip or open,

effective tensile stresses can be transmitted across this discontinuity in order to open a new crack and the hydraulic fracture will cross the natural fracture. If the interface is weak or open, it is more likely that the hydraulic fracture will divert into the natural fracture. Thus, the interface properties and cement strength are major parameters that influence the fracture crossing.

Most geomechanical modeling studies on this topic have treated natural fractures as frictional interfaces. However, based on core observation, there are abundant partially or fully cemented opening mode fractures that could be reactivated by hydraulic fracture treatments (Gale et al. 2007). The objective of this project is to investigate natural and hydraulic fracture interaction for fully cemented natural fractures.

Laboratory observation is a direct way to understand and evaluate the controlling parameters for such interactions. SCB testing is applied in this study for testing fracture toughness of samples with pre-existing natural fractures. Synthetic hydrostone sample is used to represent rock, and plaster/sandstone slice is used to represent natural fracture. Since the traditional fracture toughness calculation is defined for a homogeneous sample, we use the name "effective toughness" to describe heterogeneous sample failure (samples with pre-existing natural fractures).

The importance of hydraulic fracture approach angle in natural fracture interaction problems is studied in a series of experiments. Two types of materials with different toughness were used as inclusion, and different inclusion thickness was investigated. After completing the experiments, we analyzed the results using the ABAQUS finite element software.

1.2 Outline

This chapter includes the motivation and the project objective. Chapter 2 gives the important concepts in reservoir geomechanics and background literature review related to the project. Chapter 3 explains the experimental procedure and numerical simulation procedure. Experimental results and numerical simulation results are explained in detail in Chapter 4. Chapter 5 presents the conclusion of this study and ideas for future work.

CHAPTER 2: Literature Review

2.1 Overview

Natural gas, especially shale gas, is an abundant U.S. energy resource which plays an important role in the nation's energy demand. There is a wide distribution (Figure 2.1) of highly organic shale containing vast resources of natural gas across the lower 48 states (US DOE 2009). According to Energy Information Administration (EIA), natural gas, coal, and oil supply about 85% of the nation's energy. Out of this 85%, 26% is contributed by natural gas. The percent contribution of natural gas to the US energy supply is still slowly increasing and natural gas will continue to play a big part in the future of energy in the U.S.

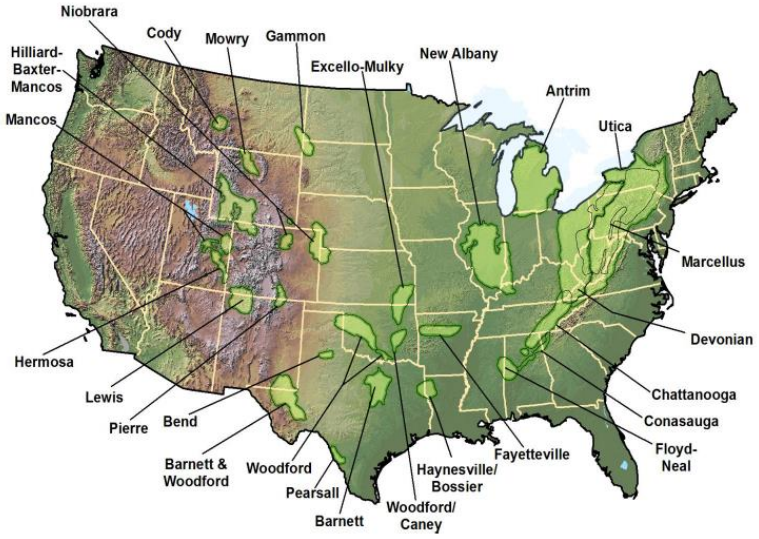

Figure 2.1: United States shale basins (from US DOE Modern shale gas development 2009).

Due to the increase of gas price and advances in technology, shale gas production is now economically viable. Hydraulic fracturing, in conjunction with horizontal drilling, is one of the most successful methods in developing unconventional resources. Proper understanding of the fracture propagation (and interaction with any fractures existing in situ) would optimize the treatment, and hence improve hydrocarbon production and reduce cost for completion.

2.2 Hydraulic Fracturing

The hydraulic fracturing technique was first introduced to the petroleum industry in July 1947, and was first applied to a gas well in the Hugoton Gas Field in Kansas by J. B. Clark (1949), while he was working for Stanolind Oil and Gas Company in Tulsa, Oklahoma. Clark published a paper that introduced "Hydrafrac", which was the basis for the current hydraulic fracturing treatment process. With technology improvements, the fracturing technique has been implemented under a wide range of conditions, from high leak-off formations to the very low leak-off tight gas formations; from low-pressure low-temperature reservoirs to high pressure, extremely low permeability deep reservoirs. Nowadays, hydraulic fracturing is extensively applied in the field to enhance oil and gas deliverability in both vertical and horizontal wells. It has been used to stimulate about 70% of the gas wells and 50% of the oil wells in the North America (Renard et al. 2008). Additionally, this technique is also applied to geothermal reservoir recovery (Robinson 1971, Harlow and Pracht 1972), CO_2 injection improvement (Leonenko and Ghaderi 2009,

Raziperchikolaee and Yin 2012), in-situ stress field measurement (Teufel and Warpinski 1983) and other applications.

During hydraulic fracturing, fluid is pumped at high pressure and high flow rate into the shale or tight gas formations to create permeable fractures. The produced fractures behave like a "highway", which allows gas that is trapped in shale pores to be able to migrate into the wellbore. The hydraulic fracture direction is predominantly controlled by the minimal principal stress direction (Hubbert and Willis 1957). Fractures open against the minimum principal stress, since it requires the least amount of energy. Principal stresses are mutually orthogonal, therefore the fracture propagates away from the well in the plane defined by the other two principal stresses. For most cases, the vertical overburden stress is the maximum stress, thus hydraulic fracturing produces vertical fractures propagating from the wellbore. However, in the case of reverse faulting regime, when the overburden stress is the minimum stress, it is also possible to produce horizontal fractures.

Hydraulic fracture jobs begin with the injection of "prepad", which is a mixture of water and low strength acid. A mixture of water, viscosifiers, and friction reducers called "pad" is injected afterwards. This is then followed by the "slurry", which is a mixture of fracturing fluid and proppant to keep the fracture open. Types of fluid and proppant are varied between different reservoirs. In the last step, the slurry inside the wellbore is displaced into the fracture (Valko and Economides 1995, Daneshy 2010).

2.3 Effects of Natural Fractures

Traditionally, fractures are described as single, bi-wing, planar crack with the wellbore in the middle of the two wings (Figure 2.2). Fisher et al. (2002) proposed a characterization method based on the complexity of the fracture network, varying from simple to complex to very complex fracture network.

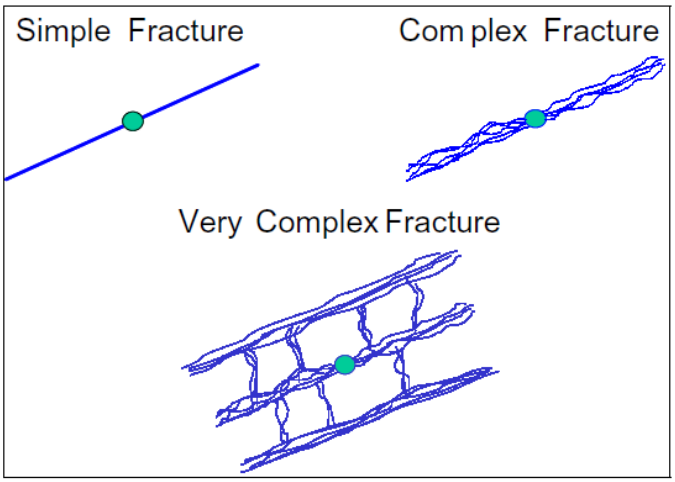

Figure 2.2. Fracture complexity (from Fisher et al. 2002).

Shale formations often contain natural fractures. The complex hydraulic facture network is strongly influenced by the interaction between hydraulic fractures and natural fractures. According to the interpretation of microseismic data (Fisher et al. 2002; Maxwell et al. 2002; Le Calvez et al. 2007), many hydraulic fracture treatments lead to complicated fracture networks. Figure 2.3 shows a plan view for a fracture structure plot from one particular treatment in Barnett shale (Fisher et al. 2002). Based on the stress state, the hydraulic fractures propagate along a north-east to south-west direction. Core data shows that the natural fractures exist sub-parallel to the fracture propagation direction and also

orthogonal to it. The micro-seismic data shows the complexity of the fracture network, it also implies that the hydraulic fracture was re-directed along some of the pre-existing natural fracture direction.

Based on the stress state, the fracture is predicted to propagate along a north-east to south-west direction. Core data shows that the natural fracture exist sub-parallel to the fracture propagation direction and also orthogonal to it.

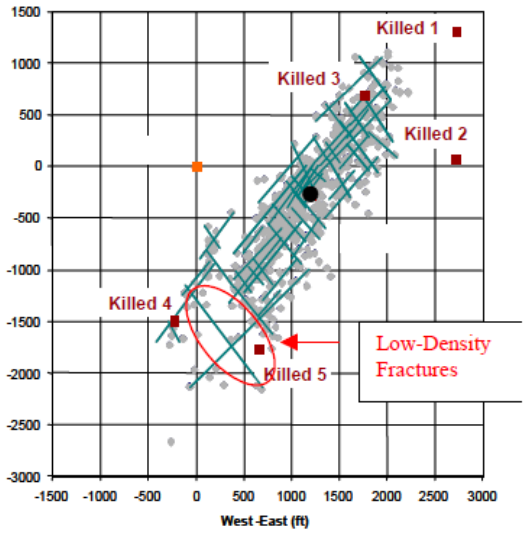

Figure 2.3: Fracture structure plot from one treatment (from Fisher et al. 2002).

The complexity of a fracture network depends on how the fractures interact with one another. However, not all natural fractures are open to flow, in some cases, when hydraulic fractures encounter natural fractures, the hydraulic fractures are arrested for further propagation (Teufel and Warpinski1987). In some other cases, for instance in the Barnett Shale, where has partially or completely cemented natural fractures (Gale et al. 2007), the hydraulic fractures are diverted into natural fractures. Therefore, a good

prediction of hydraulic fracture propagation path when there is an interaction with natural fracture could provide a better understanding of complex hydraulic fracture network. This would improve the current hydraulic fracture models for fracture propagation in a naturally fractured formation.

2.4 Interaction between Hydraulic Fracture and Natural Fracture

Most hydraulic fractures and natural fractures interaction studies treat the natural fractures as frictional interfaces with cohesion. Blanton (1982) was the first person who studied the interaction between hydraulic fractures and natural fractures. He experimented with both Devonian shale and hydrostone samples. Three types of propagation paths (Figure 2.4) were defined for the interaction:

(a) Crossing: the natural fracture has no influence on hydraulic fracture propagation. The propagating fracture will remain in the original direction and open against the minimum principal stress.

(b) Diverting: the natural fracture is opened and the propagating fracture is deflected into the open natural fracture. The natural fracture represents a weak path with less resistance. Diverting requires less energy than straight crossing.

(c) Jogging: hydraulic fracture penetrates the natural fracture by forming an offset or stepping pattern along the natural fracture.

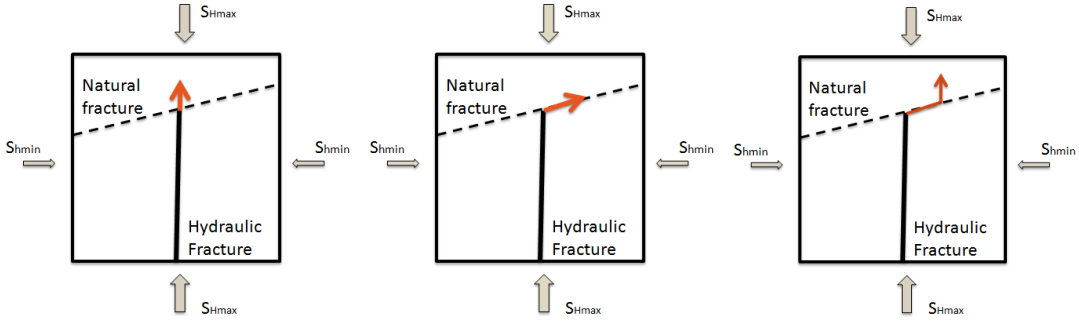

Figure 2.4: Schematic of fracture interaction: (a) Crossing; (b) Diverting; (c) Jogging.

Blanton concluded that high differential stress and nearly orthogonal approaching angle are the most important factors to promote fracture crossing. Renshaw and Pollard (1995) later developed a simple criterion for orthogonally approaching fractures. The interface is assumed to be cohesionless, and the frictional stress on the surface is assumed to obey the Coulomb law. The criterion states that compressional crossing will happen on frictional interfaces given sufficient energy to prevent slip along the interface, while at the same time the stress ahead of the fracture is sufficient to initiate a new fracture on the opposite side of the interface. Gu and Weng (2011) extended Renshaw and Pollard's (1995) criterion to non-orthogonal crossing. The crossing is determined for a given remote stress state, tensile strength, coefficient of friction, cohesion and intersection angle.

Zhang (2006) suggested that the hydraulic fractures can penetrate or cross a pre-existing natural fracture without changing direction, or may reinitiate at the site of an inherent secondary flaw to form an offset or stepping pattern. The offsetting portion is dominated by shear deformation. The new crack growth from the flaw turns to extend in

the direction by the maximum tensile stress ahead of the crack tip, which is in turn affected by the slippage of the pre-existing fracture. The pre-existing fractures can have significant effect on hydraulic fracture growth: the resulting interactions affect the fracture pressure, width, length, rate of growth and trajectory (Zhang and Jeffrey 2006).

The previous work are more focus on considering natural fractures as a frictional interface with cohesion (may be treated as the shearing mode fractures). However, for example in the Barnett shale, most natural fractures are opening mode fractures, which are commonly narrow, sealed with calcite, and present in en echelon arrays. The aperture for these cemented fractures is less than 0.05 mm. Large open fractures also exist in clusters and are spaced several hundred feet apart (Gale et al. 2007). These opening mode natural fractures could be reactivated by hydraulic fracture treatments, enhancing the formation permeability. In this report, we extend the previous work to opening mode fractures (that may be open, partially open or completely sealed). The objective for this project is to investigate natural and hydraulic fracture interaction for fully or partially cemented natural fractures.

2.5 Hydraulic Fracture Propagation

In fracture mechanics, there are three types of loading that a crack can experience as illustrated in Figure 2.5. Mode I is called the opening mode. It refers to the principal stress direction that is normal to the crack surface; therefore the fracture propagation is in the crack plane direction. Mode II corresponds to in-plane shear, fractures tend to slide between crack faces. Mode III refers to the out of plane shear. The shear displacement is

acting parallel to the front of the crack plane. A crack body can be loaded by more than one mode, this is refer to as mixed mode fracture (Anderson 2004). In this project, only opening mode fracture is considered.

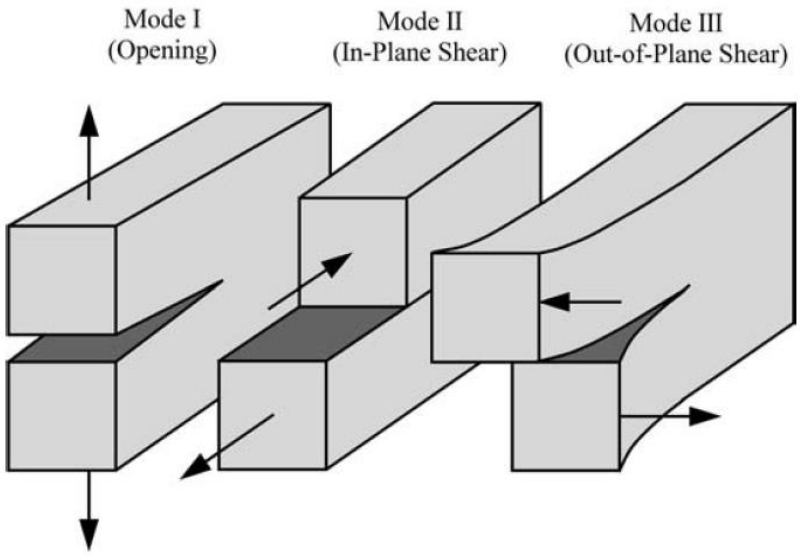

Figure 2.5: Three modes of loading that can be applied to a crack (from Anderson 2004).

Linear elastic fracture mechanics (LEFM) is often applied for analyzing crack propagation in rock mechanics. When the stress near the crack tip exceeds the material fracture toughness, the crack will propagate. Rock fracture toughness depends on the rate of loading, but not the thickness or sharpness of the crack tip (Haberfield and Johnston 1994). It is also independent of the specimen thickness, specimen size, grain size, and notch length (Park et al. 2004, Lim et al. 1994). In LEFM, the process zone represents a volume around the crack tip where energy is dissipated by ductile strain or micro-cracking and

shear (Whittaker et al. 1992). As long as the process zone energy is small enough, linear elastic fracture mechanics can be applied. Thiercelin and Roegiers (1986) suggested applying compressive stress normal to the crack surface could create a smaller process zone using modified ring test, which is also applied to semi-circular bending test.

The *stress intensity factor* (K) is the most important concept in fracture mechanics. It defines the crack tip condition. The fracture will propagate when stress intensity factor is above the critical value (K_C). K_C represents the fracture toughness, which is a rock property (Anderson 2004). This is the propagation criterion when there is no chemical weakening effects that may cause subcritical crack growth (Atkinson 1989).

Another important parameter is the *energy release rate* (G), which was first introduced by Irwin in 1965. It describes the rate of change in potential energy near the crack area for a linear elastic material. When the energy release rate (G) reaches the critical value (G_c), the crack will propagate. In LEFM, the energy release rate is described by the path-independent J-integral (Rice 1968):

$$J = \int_{\Gamma} \left(\omega dy - T \frac{\partial u}{\partial x} ds \right) \qquad (1)$$

where ω=strain energy density,

T=traction vector,

u=displacement vector, and

ds=length increment along the contour Γ.

For a mixed mode crack that propagates in its own plane, the energy release rate (G) equals to the J-integral and is related to the stress intensity factor (K) as:

$$G = J = \frac{(K_I^2 + K_{II}^2)}{E^*}; \qquad (2)$$

where $E^*=E/(1-\nu)$ for plane strain, E is Young's modulus and ν is Poisson's ratio.

The fracture will choose the direction (θ_o) that has the highest energy release rate ($\overline{G}$), and the initiation occurs when energy release rate reaches a critical value (G_c) (Nuismer 1975).

$$\overline{G} = \frac{(k_I^2 + k_{II}^2)}{E^*} \geq G_c; \qquad (3)$$

$$k_I = \frac{1}{2}\cos\left(\frac{\theta_o}{2}\right)[K_I(1+\cos\theta_o) - 3K_{II}\sin\theta_o]; \qquad (4)$$

$$k_{II} = \frac{1}{2}\cos\left(\frac{\theta_o}{2}\right)[K_I\sin\theta_o + K_{II}(2\cos\theta_o - 1)]; \qquad (5)$$

K_I and K_{II} represents the stress intensity factor for in-plane propagation ($\theta_o=0^\circ$), and k_I and k_{II} account for propagation in a general direction, θ_o.

For the case of fracture intersection in rocks, G_c^{frac} is used to represent the energy required to open a cemented fracture. The cemented fracture can be opened through the bonding interface or within the fracture cement. G_c^{rock} represents the energy to break intact rock. If there is more than 1 path for the fracture to follow, the fracture will choose the one with the higher ratio of G/G_c (Dahi-Taleghani and Olson 2009).

Figure 2.6 shows the values of k_I and k_{II} for Mode I loading, which are normalized with the maximum stress intensity factor K_I. The energy release rate (green dot curve) is changing with different fracture propagation directions. For a mode I fracture (K_{II}=0), the highest energy release rate occurs at θ_o=0˚, and the lowest energy release rate occurs at θ_o=±180˚. Thus, for the case of a homogeneous material when a fracture starts to propagate, it will go straight because the energy release rate is the highest. For the case where a propagating fracture hits the natural fracture at a 30˚ angle, if the energy release rate ratio, G/G_c^{frac}, inside the fracture is higher than the energy release rate ratio. G/G_c^{rock}, for the intact rock, fracture will divert along the natural fracture. If diversion occurred, the fracture would divert into the 30˚ direction rather than the 150˚ direction, since the smaller angle has a higher energy release rate.

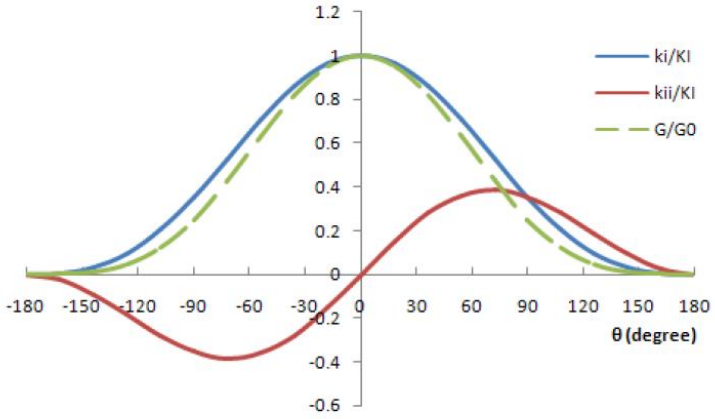

Figure 2.6: Energy release rate for different propagation directions for Mode I loading regime (from Dahi-Taleghani 2009).

2.6 Semi-Circular Bending (SCB) Test

Laboratory experiments are a direct and effective way to observe fracture crossing/diverting behavior, with the advantages of repeatability. In fluid driven hydrostone experiments, oblique cemented natural fractures are more likely to divert propagating fractures in comparison to the natural fractures that are orthogonal to the hydraulic fracture path (Blanton 1982, Gu and Weng 2011, Olson et al. 2012). The angle of approach is only one of the factors determining the behavior. For an orthogonal approach angle, the hydraulic fracture is more likely to cross the natural fracture under high normal confining stress and arrest under low normal confining stress (Meng and Pater 2011). The block tests give very insightful results because of the similarity to real hydraulic fracture job in the field. However, hydraulic fracture tests done with real rock blocks will require a lot of subsurface rock sample, which can be very expensive. Besides, most natural rocks have heterogeneous characteristics, which made them difficult to confidently interpret the laboratory results. Thus, if an alternative test approach could be developed and useful information can be extracted, it would be very beneficial in further understanding of the fractures interaction problem.

The alternative, simpler approach we propose is the semi-circular bending (SCB) test. Semi-circular bending (SCB) test was first proposed by Chong and Kuruppu (1984) to evaluate Mode I fracture toughness. This method only requires the use of compressive load, and has been used for a broad range of rock types. Semi-circular specimen uses only half of the sample size comparing with the conventional Brazilian tensile test sample, which makes it cost effective and easy to handle (Park et al. 2004). Besides, this experiment

demonstrated equally reliable results as the previous testing method of SECB (single edge cracked beam) and SECRBB (single-edge cracked round bar bend) (Lim et at 1994). Thus, semi-circular bending test is used to measure fracture toughness in this project. In this research, hydrostone was chosen to be the test material, because it is homogeneous, isotropic, and the mechanical properties can be easily altered by varying the hydrostone mixture (Blanton 1982). Two types of inclusion materials with different toughness are used to assess their effect on fracture propagation. Additionally, the orientation and thickness of the inclusion are also evaluated in a series of experiments.

One of the main disadvantages of SCB testing is inability to incorporate confining stress. Thus the results of this work have to be completed by a numerical method. We next overview most common methods used in solid and fracture mechanics.

2.7. Finite Element Method and Associated Numerical Approaches

Many problems in engineering and science are dealing with complicated geometries, properties and boundary conditions, which make the usage of exact, closed-form solution impossible. The finite element method (FEM) is one of the techniques to obtain approximate solutions to many problems that encountered in engineering analysis, while the analytical solutions are not available (Barton and Rajan 2000). Originally, the FEM was used to solve complex elasticity and structural analysis problem in civil and aerospace engineering, and it becomes a very popular methodologies in rock mechanics related problems (Anderson 1968).

FEM was first developed in 1943 by R. Courant, who utilized the Ritz method of numerical analysis and minimization of variational calculus to obtain approximate solutions for vibration systems. Shortly thereafter, a paper published in 1956 by M. J. Tumer, R. W. Clough, H. C. Martin, and L. J. Topp established a broader definition of numerical analysis (from http://www.sv.vt.edu/classes/MSE2094_NoteBook).

Most commercial FEM software packages originated in the 1970s (ABAQUS, ADINA, ANSYS, MARK, PAFEC) and 1980s (FENRIS, LARSTRAN, SESAM). The FEM is one of the most important developments in computational methods to occur in the 20^{th} century. Nowadays ABAQUS, ADINA, ANSYS, FRANC3D are the best known finite element software packages (Barton & Rajan 2000).

In this report, ABAQUS is used for numerical simulation. ABAQUS is a suite of powerful engineering simulation programs, which can solve problems ranging from relatively simple linear analyses to the most challenging nonlinear simulations. It can be used to study more than just structural (stress/displacement) problems, but also simulate problems that involve mass diffusion, soil mechanics, and fluid dynamics and so on (ABAQUS 6.13 Documentation). A detailed explanation about numerical simulation procedure is provided in Chapter 3.

CHAPTER 3： Experimental and Numerical Simulation Procedures

In this chapter, the experimental preparation and setup are discussed. The numerical model that is used to simulate problems is explained in detail. Subsequently, a simple model validation and sensitivity analysis are presented.

3.1 Experimental Materials

The synthetic samples used in this project are composed of hydrostone matrix and plaster/sandstone inclusion. The inclusion represents the pre-existing, cemented natural fracture. The hydrostone is a mixture of gypsum and cement, which is produced by United States Gypsum Company (IG-123-F1-50BAG/6-99), and the gypsum plaster is made by DAP Products Inc. (55FG-DAP-135094A). The ratio for mixing powder and water is given in the Table 3.1.

Material	Dry cement weight, %	Water weight, %
Hydrostone	75.7	24.3
Gypsum plaster	63	37

Table 3.1: Hydrostone and plaster mixing percentages.

The well-mixed liquefied gypsum is poured into a rectangular shape mold and is fully cured at room temperature. A low-speed saw is used to slice the gypsum and sandstone blocks to desired length and thickness. Then the gypsum/sandstone slice is put into a semi-circle shape mold. The bottom and side of the mold are sealed by tape, so the

slice would be held in place before liquid hydrostone is poured. The last step is to pour the well-mixed liquid hydrostone into the mold.

The Young's modulus and UCS for hydrostone and plaster are a function of curing time. The Young's modulus rises from 50,000 psi the 1st day to 200,000 psi the 4th day and remains unchanged after 15 days. The UCS rises from 200 psi to 1000 psi within this period and keeps the same (Bahorich 2012). Thus, the prepared hydrostone samples are set in room temperature for 4 days until they are fully solidified.

The semi-circle sample is then polished with sand paper to remove any irregularities. The inclusion's position, thickness, and strength are varied as presented in Figure 3.1. The SCB test is performed on samples to test the effective toughness and observe the fracture propagation path.

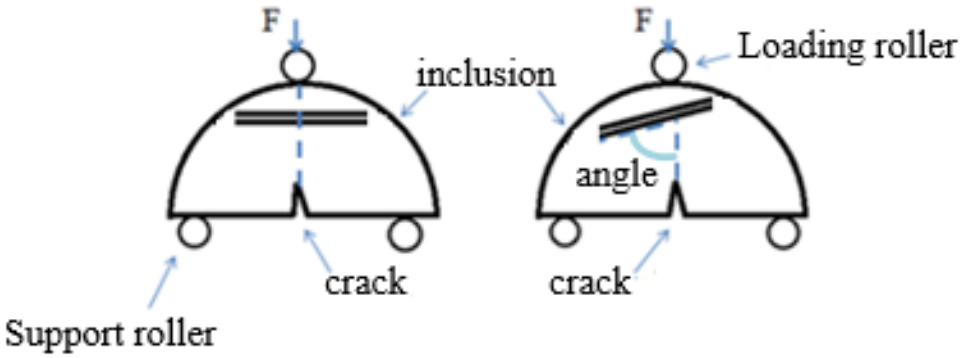

Figure 3.1: Schematic view for SCB samples with inclusion placed at different angles.

Two sample sizes were prepared for SCB test, a large sample with a 3-in diameter and 1-in thickness, and a small sample with a 1.55-in diameter and 0.6-in thickness (Figure 3.2).

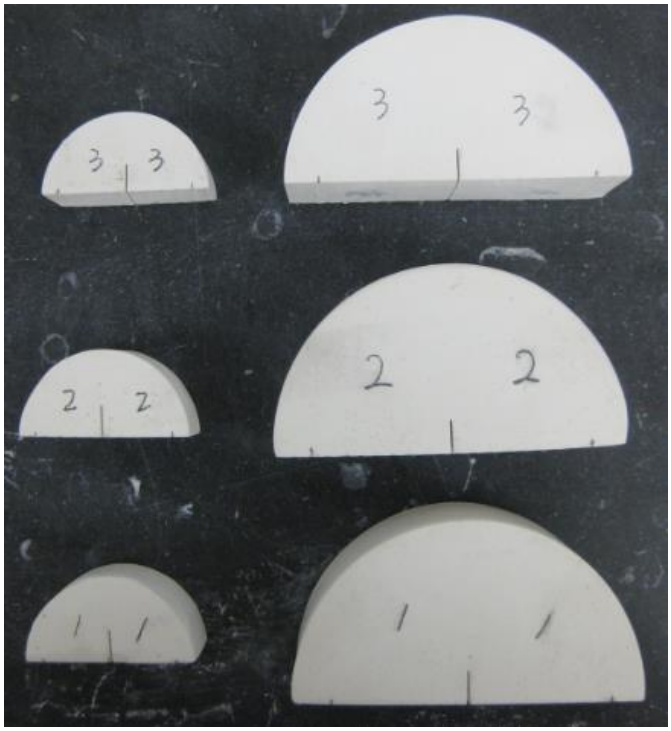

Figure 3.2: Hydrostone samples before testing.

The elastic properties are given in Table 3.2 (Bahorich 2012, Teufel 1984). Compared with hydrostone, plaster has a similar Young's modulus, but a relative low tensile strength and unconfined compressive stress (UCS). Thus plaster represents a weak inclusion. Berea sandstone has a higher Young's modulus and strength, so it represents a strong inclusion.

Material	E (psi)	Tensile strength (psi)	UCS (psi)
Hydrostone	≈ 200,000	700	3,000 ~ 5,000
Plaster	≈ 200,000	300	1,000
Berea sandstone	377,000	625.5	11,600

Table 3.2: Elastic properties for hydrostone, plaster and Berea sandstone.

3.2 Experimental Procedure

Figure 3.3.a shows the schematic view of the SCB test. Figure 3.3.b shows the experimental setup in the lab. The sample is loaded by applying a constant displacement rate of 0.003 in/min.

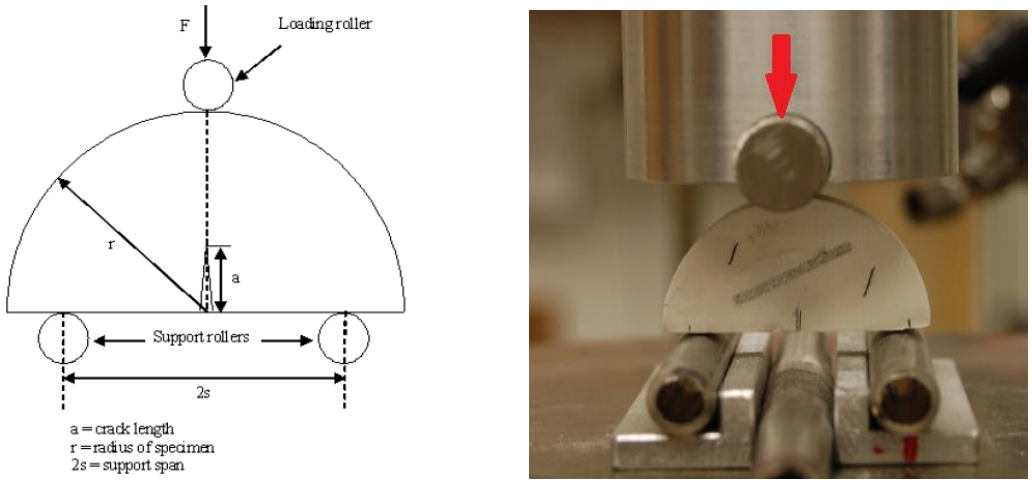

(a) (b)

Figure 3.3: (a) Semi-circular bending test specimen schematic (Park et al. 2004);

(b) Experimental setup for SCB test in the lab.

For the SCB test, pure Mode I loading is obtained when the notch is perpendicular to the base of the sample. The fracture toughness (K_{IC}) is calculated as

$$K_{IC} = \frac{P\sqrt{\pi a}}{DB} Y_I \qquad (1)$$

where P is the peak load, a is the notch length, D is the sample diameter, and B is the sample thickness. Y_I is a dimensionless coefficient which based on regression analysis (Lim et al., 1993):

$$Y_I = 4.782 - 1.219\left(\frac{a}{r}\right) + 0.063\exp\left(7.045\left(\frac{a}{r}\right)\right) \qquad (2)$$

The SCB specimens used in this study are constrained to $0.03 \leq a/r \leq 0.8$, and s/r = 0.8 (Lim et al 1993, Park et al 2004). The average fracture toughness (K_I) for hydrostone was determined to be 0.42 MPa$\sqrt{m}$, and for plaster it was 0.185 MPa$\sqrt{m}$. These values are used for comparison with hydrostone samples with plaster inclusion.

3.3 Numerical Simulation Procedure

Finite element software ABAQUS is used for numerical analysis in this project (ABAQUS Documentation 6.13). ABAQUS is known as a high quality performance program, which is designed primarily to model the behavior of solids and structures under externally applied loading. It could model complicated interface between solids, and it also has the capability to model various phenomena of interest, including structure interactions, and fluid flow.

A homogeneous hydrostone sample with a radius of 0.725 in and initial crack length of 0.24 in was built first (Figure 3.4). The elastic properties are E = 1.38GPa, and ν = 0.28.

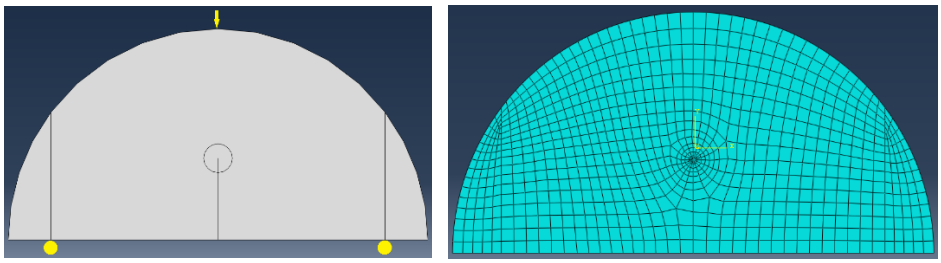

(a) (b)

Figure 3.4: Hydrostone sample geometry (a) and mesh (b).

In SCB test, the maximum applied load for homogeneous hydrostone is 72.5 lb. This concentrated load is applied on top of the sample in ABAQUS. There are two support rollers on the bottom which restrict displacement in the y-direction. In order to perform the contour integral analysis in ABAQUS, the crack front, crack tip and crack extension direction need to be specified in the "Interaction" module. The crack is modeled as an embedded line that contains edges that are free to move apart from each other (without having a mesh element in between). In other words, when meshing the model, ABAQUS creates duplicate overlapping nodes on the crack line. These nodes are free to move apart as the crack separates. A global seed size of 1.0 is assigned to the part. 16 elements local edge seed is assigned along the circular region surrounding the crack tip. Additional constraint is applied to make sure the number of elements along this edge may only increase, and this constraint will improve the mesh quality in this case. 4 elements local edge seed is assigned along the straight edge within the circular region. No additional constraint is required here. The intact and deformed shapes are shown in Figure 3.5.

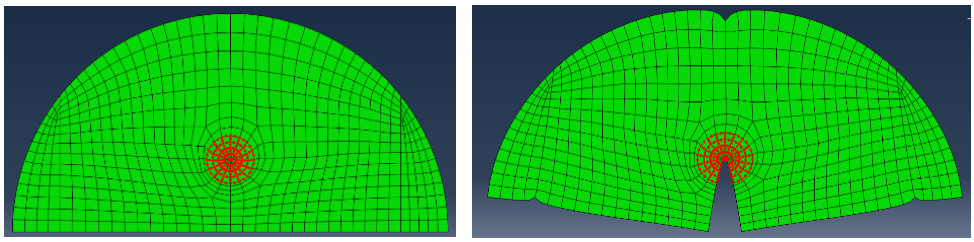

(a) (b)

Figure 3.5: Intact (a) and deformed (b) SCB model.

Swept mesh control is assigned to the circular region. The mesh is generated from the crack tip in a radial fashion over the circle. Free Quad element shape is assigned to the rest of the region, and the medial axis algorithm is selected. Quadratic, reduced integration plane strain elements (CPE8R) are assigned to all regions of the SCB model.

Figure 3.6 shows the von Mises stress distribution in the sample. In engineering related problems, the von Mises stress is used to display the yielding area. Figure 3.6 indicates the stress state is highly localized in the vicinity of the crack tip, loading point and two supporting points. Five contour integral values are calculated next to the crack tip. The contour domain is identified in Figure 3.7. Each successive domain contains the previous domain within its boundaries.

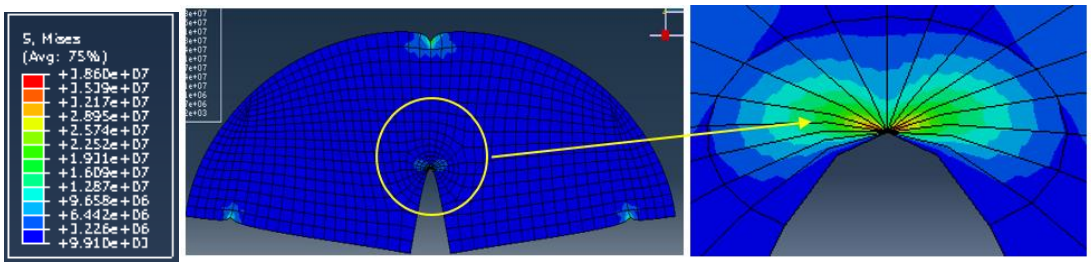

(a) (b)

Figure 3.6: Von Mises stress distribution that corresponds to the deformed sample in Figure 3.5.

The calculated stress intensity factor for each contour is shown in Figure 3.7. Even though the differences in the value of K for each contour appear to be small, the first contour value is neglected to prevent adverse numerical effects due to singularity from influencing the interpretation of the results. Thus, the average value of K_I for contour 2-5 is 0.417 MPa$\sqrt{m}$. The effective toughness value from the numerical simulation is close to the experimental result, which is 0.42 MPa$\sqrt{m}$. The difference is about 0.7%.

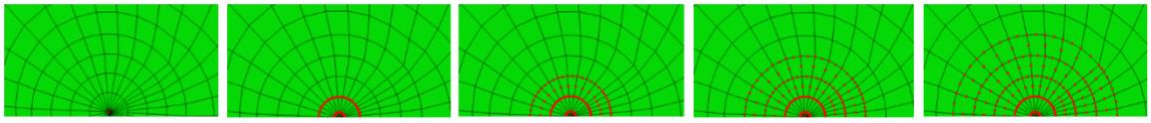

CRACK NAME	CRACKFRONT NODE SET	C O N T O U R S				
		1	2	3	4	5
H-OUTPUT-2_CRACK-1						
-7-	K1:	4.1711E+05	4.1688E+05	4.1699E+05	4.1701E+05	4.1699E+05
	K2:	35.14	61.32	71.21	91.59	92.87
MTS	DIRECTION (DEG):	0.000	-1.6856E-02	-1.9569E-02	-2.5169E-02	-2.5522E-02
	J from Ks:	116.3	116.1	116.2	116.2	116.2

Figure 3.7: Contour integral domain and output results.

According to Lim et al.'s equation (Equation 1), if the load P is fixed, the stress intensity factor (K_I) increases as the initial crack length (a) is increasing. Since Lim et al.'s equation is only valid for a/r in the rage of 0.03 to 0.8 (Lim et al. 1993), the ABAQUS model is performed in the range of 0.127 to 0.762. The overall numerical simulation result matches the analytical solution very well (Figure 3.8) except for the model with a very small initial crack length (a). When the initial crack length is small, there is a big difference between each contour integral, which indicates that the mesh quality is low, therefore a refined mesh is required.

	K, (MPa*m^0.5)											
a/r	0.127	0.191	0.222	0.254	0.318	0.381	0.445	0.484	0.508	0.572	0.635	0.762
Equation (Lim et al. 1994)	0.194	0.237	0.256	0.275	0.311	0.347	0.388	0.417	0.436	0.499	0.581	0.859
ABAQUS	0.077	0.059	0.202	0.252	0.297	0.337	0.383	0.417	0.439	0.508	0.596	0.860
Error, %	60.40	75.21	20.97	8.45	4.65	3.00	1.22	0.04	0.77	1.85	2.54	0.17

Table 3.3: Stress intensity factor comparison for different crack length.

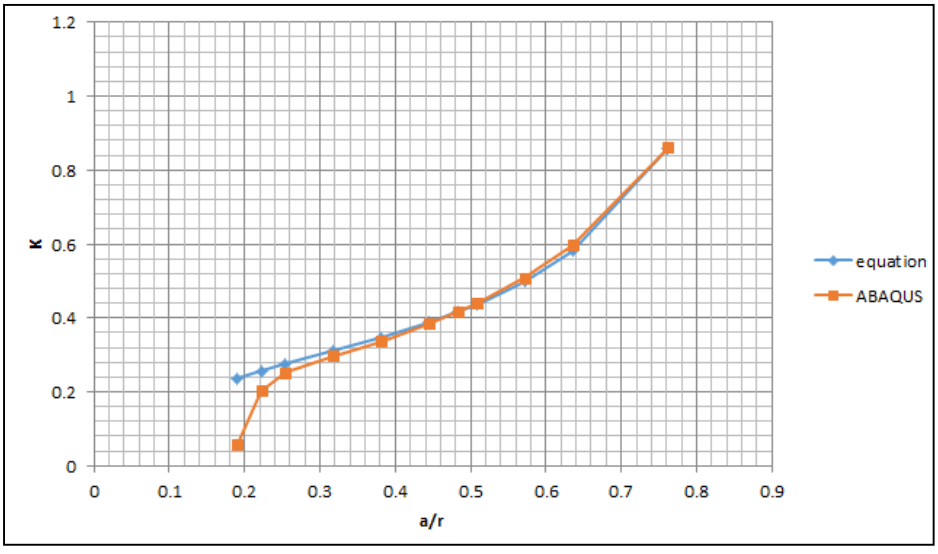

Figure 3.8: Stress intensity factor comparison for different crack length.

Given this validation of the numerical model for the homogeneous case, we are able to move to samples with an embedded inclusion and conduct the simulation to get some results.

An inclusion slice (0.05 in thickness) is embedded into the previous hydrostone sample (Figure 3.9). For the interface between hydrostone and plaster, a friction coefficient value 1.06 is set for the tangential behavior (Bahorich 2012). For the normal behavior, a "hard contact" is defined. Both the plaster and the sandstone were used as inclusion materials in the simulation. The material properties are listed in Table 3.2. Plaster represents a weak inclusion and sandstone represents a strong inclusion. Boundary conditions are kept the same as the homogeneous sample. In order to simulate the fracture propagation, fracture is manually cut from the initial crack length of 0.24 in until it reaches the embedded inclusion.

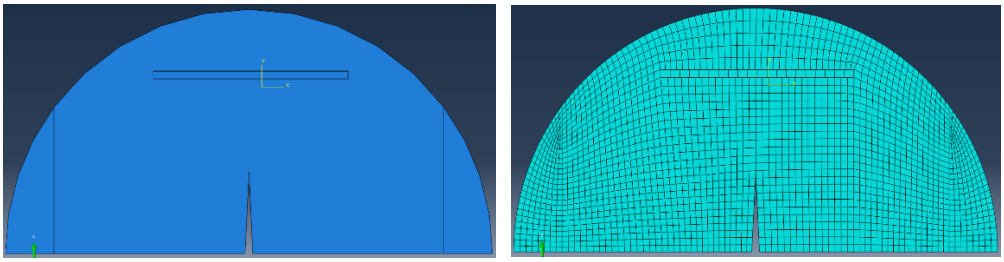

(a) (b)

Figure 3.9: a) Hydrostone sample with embedded inclusion, b) corresponding mesh.

A sensitivity analysis for the number of mesh elements in the inclusion was conducted. Since we are interested in the rock-inclusion interface behavior, S_{xx} value for

three nodes on the lower interface ahead of the crack tip are tracked for different mesh density of the inclusion (Figure 3.10).

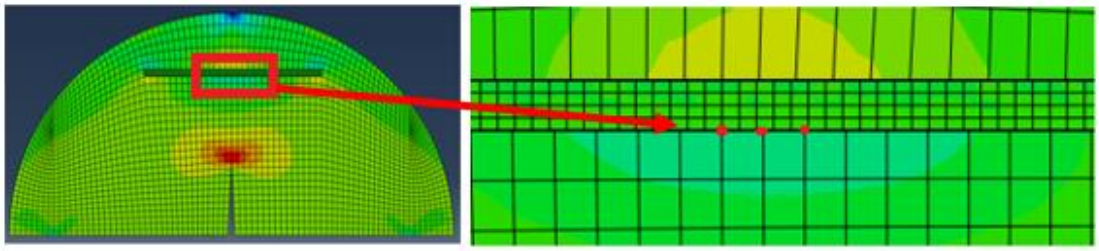

Figure 3.10: Simulation result for stress in the x-direction (S_{xx}).

Figure 3.11 shows the sensitivity analysis result. The x-axis in Figure 3.11 represents the three nodes on the interface, the y-axis in Figure 3.11 represents the stress state for each node. L indicates the number of mesh elements in the x-direction (Figure 3.11). The number of mesh elements is varied from 20 to 80. This is significant variation in results going from 20 to 70 elements, but from 70 to 80 the results only change slightly. Stable stress state indicates the simulation result is independent of mesh density. Thus, we choose the number of mesh elements in the x-direction to be 70. The same sensitivity analysis is applied to the y-direction, and we choose the number of mesh elements in the y-direction to be 3 (Figure 3.12). The simulation results are compared with experimental results and are discussed in detail in Chapter 4.

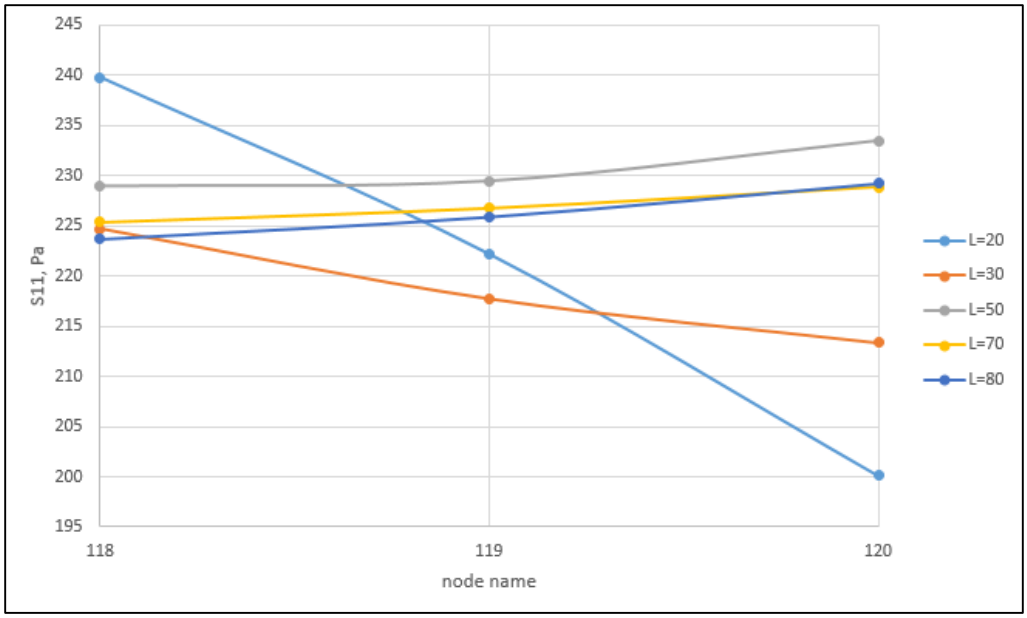

Figure 3.11: Stress state of each node for different mesh density (x-direction).

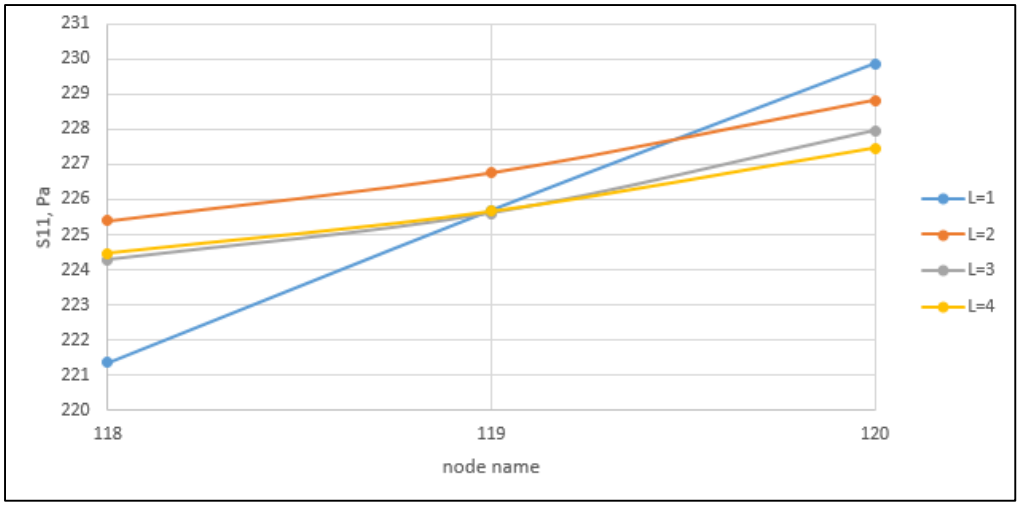

Figure 3.12: Stress state of each node for different mesh density (y-direction).

CHAPTER 4: Results and Discussion

This chapter shows the SCB test results on hydrostone and mudstone samples with different inclusions and approach angles. The propagating fracture typically crosses (Figure 2.4) the inclusion for orthogonal or high degree approach angles. The crossing surface is not a clean cut, but with a jog distance. At low approach angles, the fracture is usually diverted along the inclusion. Rather than a clean crossing surface, jogging or short offset along the inclusion, is observed for samples with 90° approach angle.

4.1 Approach Angle and Inclusion Strength Effects

The strongest observed influence on crossing versus diversion is the approach angle (Figure 4.1). The inclusion thickness for these tests is 0.05 inch. The crossing surface is not a clean cut, but with a jog distance depending on the inclusion thickness and approach angle. Detailed explanation could be found later. For sample with a 90° approach angle, most of the propagating fractures crosses inclusions (about 90 to 100% of the 5-10 samples tested in each round). At a 60° approach angle, only 40-67% of the cases result in fractures crossing inclusions. With a 30° approach angle, all propagating fractures divert into inclusions (Table 4.1).

(a)

(b)

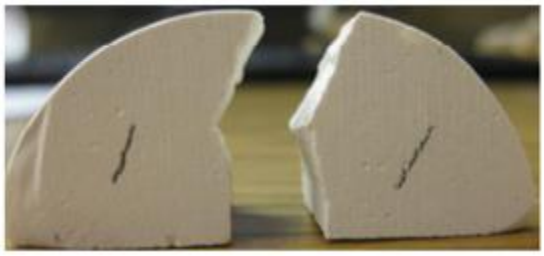

(c)

Figure 4.1: Sample at the end of test. Propagating fracture was approaching inclusion with angle (a) 90°; (b) 60°; (c) 30°.

Tests were run for both the weak inclusion (plaster) and the strong inclusion (Berea sandstone), and the results are consistent. However, it is interesting to see that for the 60° approach angle cases, the stronger sandstone inclusion has a lower crossing percentage than the plaster inclusion. For both hydrostone and plaster samples, as the approach angle decreases, the effective toughness also decreases, which indicates that a lower energy is required to initiate the propagation when the fracture and the inclusion are close to parallel.

When compared with the weak plaster inclusion samples, the strong sandstone inclusion samples have higher effective toughness.

According to literature, the permeability for gypsum plaster is 57.3 md (Bahorich 2012), and the porosity is 0.3 (Bayne 2004). Berea sandstone has permeability as 300 md, and porosity about 0.22 (Garg et al. 1996). Using Carman-Kozeny equation (1), we are able to roughly estimate the grain size for Berea sandstone is about 55.2 micron and gypsum plaster is about 13.6 micron. By visual observation, it can also be seen that the Berea sandstone's surface is rougher than the plaster's surface.

$$k = \frac{\phi^3 D_p^2}{72\tau(1-\phi)^2}; \quad (1)$$

where k: permeability;

D_p: grain diameter;

τ: tortuosity. It equals to 2.5 for dense packing object;

ϕ: porosity.

This would result in a larger surface area and a better cohesion for samples with Berea inclusion. Thus, a higher energy is required for fracturing.

Angle	90°		60°		30°	
Inclusion	Plaster	Sandstone	Plaster	Sandstone	Plaster	Sandstone
No. of sample tested	9	5	6	10	8	5
Percentage of crossed sample	89%	100%	67%	40%	0%	0%
Effective toughness (K_{IC})	0.44	0.585	0.436	0.493	0.32	0.36

Table 4.1: SCB test results for samples with plaster/sandstone inclusion. For definition of crossing refer to beginning of Section 4.1 and Figure 2.4.

Another observation is that the crack often breaks along the rock and inclusion's interface. As the propagating fracture reached the inclusion, instead of propagating inside the inclusion, the interface debonded (Figure 4.2). This phenomenon indicates that the bonding between the matrix and the inclusion is the weakest part of the SCB samples. Bahorich (2012) measured the fracture toughness by using a 0˚ approach angle: the plaster-plaster bond was 0.1 MPa$\sqrt{m}$, and the Berea-plaster bond was 0.09 MPa$\sqrt{m}$. His results (Bahorich 2012) indicate the interfacial bonding strength is a lot lower than the sample's effective toughness, which would be the reason causes interfacial open.

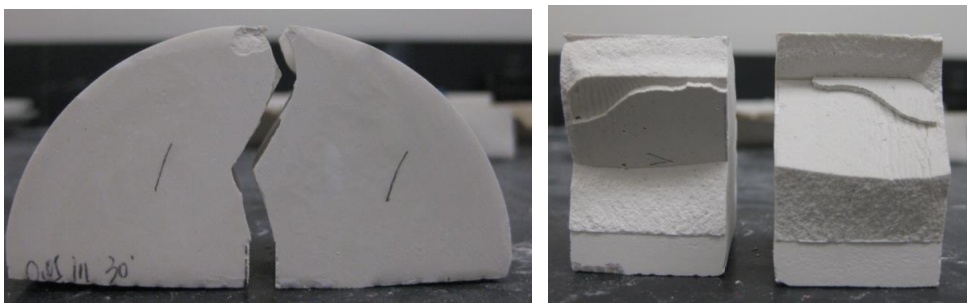

(a) (b)

Figure 4.2: SCB sample after testing, fracture propagated along the interface.

4.2 Inclusion influences the fracture propagation direction

The fracture propagation path in Figure 4.3 shows a curved crack path for the propagating fractures that approached the inclusion at both the 30° and 60° cases.

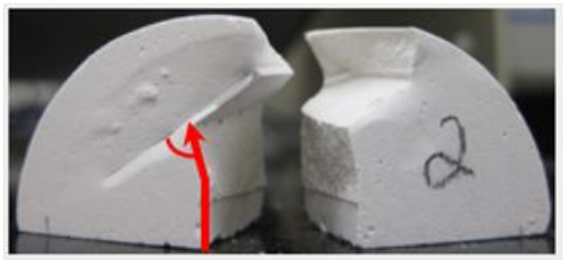

(a)

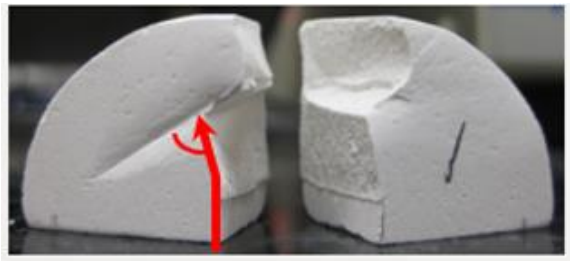

(b)

Figure 4.3: Continued to next page.

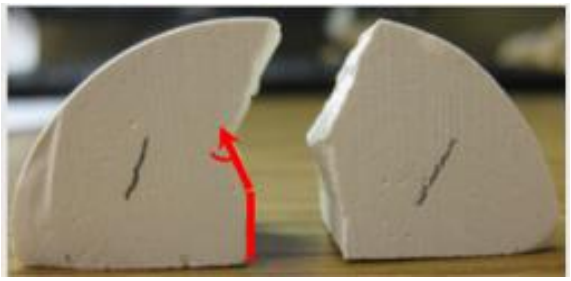

(c)

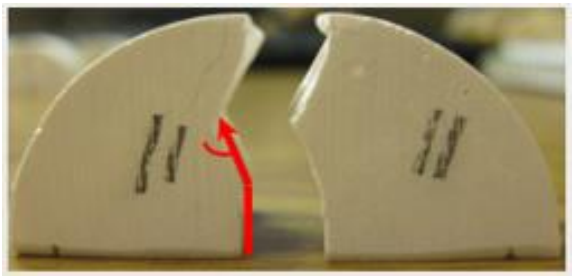

(d)

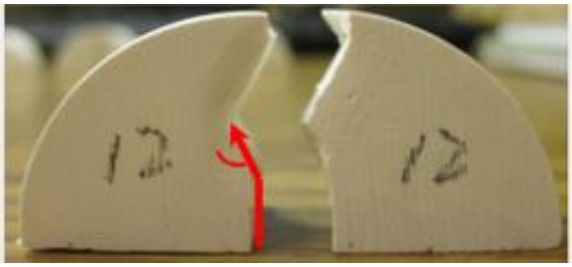

(e)

Figure 4.3: SCB samples after testing, propagating fracture curved toward inclusion for samples with approaching angle (a) (b): 60˚; (c)-(e): 30˚.

A 0.03 inch vertical notch is cut before testing. Notch is oriented to have an approach angle of 60˚, however, as the crack propagating toward the inclusion, it curves to make the approach more orthogonal, reaching about 70˚. For samples with 30˚ approach angle, the final angle is between 50˚-70˚.

In order to better understand the experimental results, finite element software ABAQUS is used for detailed stress/strain calculation. The maximum shear stress plot indicates that as fracture starts propagating from step 1 to step 2 (Figure 4.4), there is a high shear stress zone around the crack tip that appears tilted as if trying to orthogonally meet the interface, which makes the fracture curve towards the inclusion.

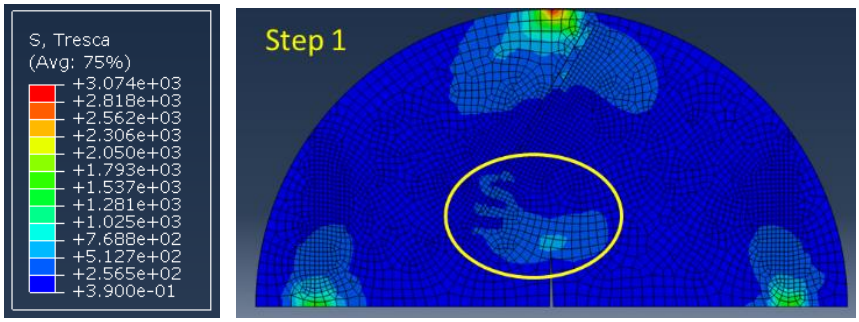

(a)

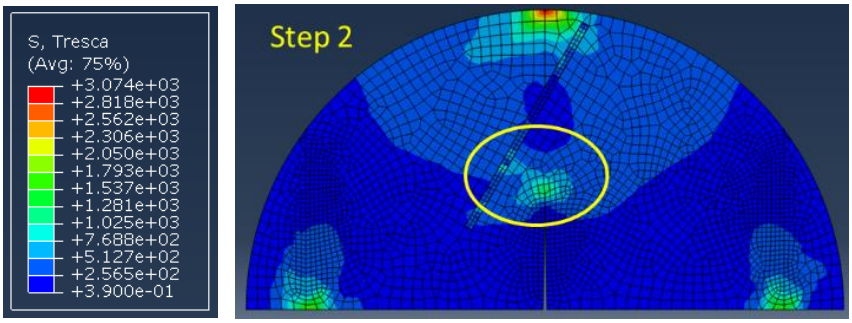

(b)

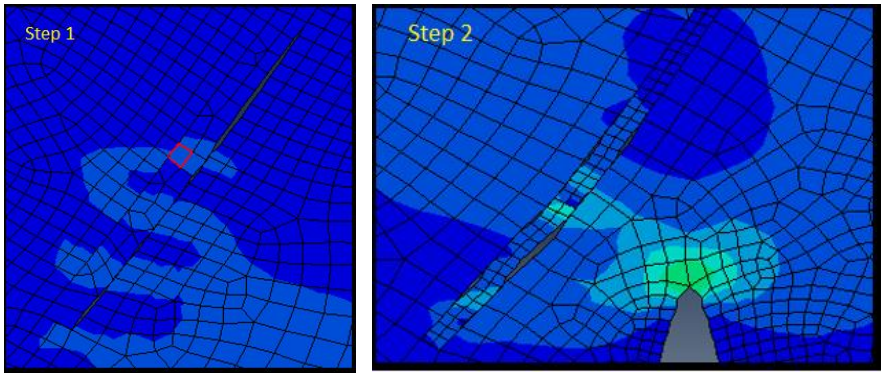

(c) (d)

Figure 4.4: Maximum shear stress contour plot for SCB sample with 30˚ approach angle.

From the maximum shear stress plot, it is also observed that there are high shear stress regions inside the inclusion. This region occurred either on the top portion of inclusion or on the lower portion of inclusion, which indicates a high potential of shear breakage. This breakage is also observed in the lab experiment when the fracture diverts along the rock-inclusion interface. The diverted fracture typically breaks across the inclusion after the initial interfacial diversion.

Figure 4.5 shows the results for samples with 30˚ approach angle, breakage occurred either on the lower part of the inclusion (Figure 4.5.a) or on the upper part of the inclusion (Figure 4.5.b). For 30˚ approach angle samples, diversion happens all the way to the end of the inclusion.

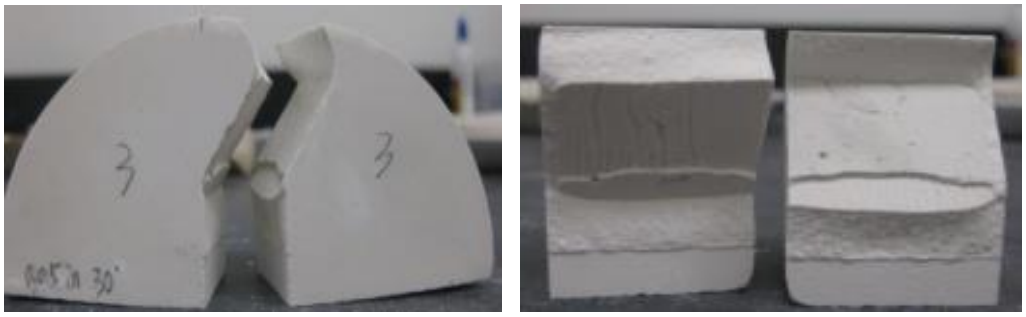

(a)

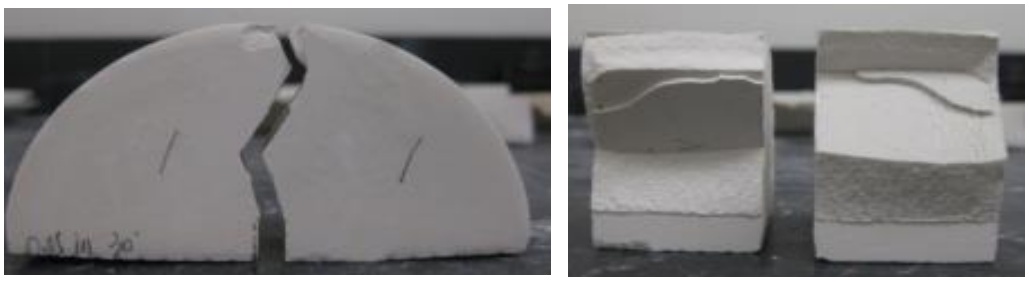

(b)

Figure 4.5: Propagating fracture diverts into the plaster inclusion and breaks the inclusion for approach angle of 30°.

For 60˚ approach angle samples, there is about a 30% chance for propagating fracture to divert into the plaster inclusion. Figure 4.6 shows the diversion results. Similar to 30˚ approach angle samples, the propagating fracture diverts into the hydrostone-plaster interface and breaks the plaster inclusion. The breakage also happened on both the lower part and the upper part, but the lower part has a relative larger diversion distance. The maximum diversion distance for 60˚ approach angle samples varies from 0.08 in to 0.15 in. It is also observed that, instead of diverting all the way to the end of the inclusion, the diversion only happened on part of the inclusion length.

(a)

(b)

Figure 4.6: Continued next page.

(c)

(d)

Figure 4.6: Propagating fracture diverts into the plaster inclusion and breaks the inclusion for approach angle of 60˚.

It has been shown that in the case of propagating crack intersects with natural fractures, and where a crack has more than one path to follow, the fracture would choose the path that has the greatest relative energy release rate, which is G/G_c (Freund and Suresh 2003, Dahi-Taleghani 2011). For the SCB sample with a 30˚ approach angle, when the propagating fracture (red arrow in Figure 4.7) hits the inclusion (blue dotted line in Figure 4.7), there is more than one path available for fracture propagation: straight (Path 2 in Figure 4.7), 30˚ to the right (Path 1 in Figure 4.7) and 150˚ to the left (Path 3 in Figure 4.7).

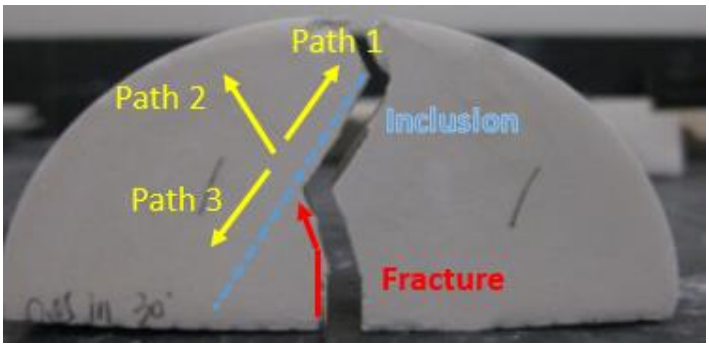

Figure 4.7: Sample with 30˚ approach angle after SCB test.

According to the homogeneous SCB test results, the stress intensity factor for homogeneous hydrostone was 0.42 MPa$\sqrt{m}$ and for plaster was 0.1 MPa$\sqrt{m}$ (Bahorich 2012). Based on the elastic properties from Chapter 3 Table 3.2, the energy release rate for hydrostone and plaster can be calculated as

$$G_c^{\text{hydrostone}} = \frac{K^2}{E^*} = \frac{K^2(1-\nu^2)}{E} = \frac{0.42^2 * (1-0.28^2)}{1379} MPa.m = 118 \frac{J}{m^2}$$

$$G_c^{\text{plaster}} = \frac{K^2}{E^*} = \frac{K^2(1-\nu^2)}{E} = \frac{0.1^2 * (1-0.28^2)}{1379} MPa.m = 6.68 \frac{J}{m^2}$$

The energy release rate for the plaster inclusion is lower than the energy release rate for the hydrostone rock. Thus, the plaster inclusion has a greater relative energy release rate (G/G_c) which makes the fracture diverting rather than propagating straight.

There are two paths available for the diversion case: 30˚ direction and 150˚ direction (yellow arrows in Figure 4.7). According to Figure 2.6 (from Dahi-Taleghani 2011) in Chapter 2, the 30˚ path has the relative energy release rate (G/G_c) about 0.9, and the 150˚ path has the relative energy release rate (G/G_c) about 0.02. Thus, the fracture will divert into the direction of 30˚ instead of 150º, because the higher relative energy release

rate occurs at a 30˚ angle. The theoretical prediction (Dahi-Taleghani 2011) are consistent with SCB test results for samples that have 30˚ approach angle.

4.3 Inclusion thickness effect and fracture jogs

A series of samples with different inclusion thicknesses and a 90° approach angle are tested (Figure 4.8). Results show that most of the hydraulic fractures crossover the inclusion regardless of the inclusion's thickness. However, the crossing is not entirely clean. The fracture typically jogs slightly at both the top and bottom interfaces of the inclusion. It is observed (Figure 4.8) that for thick inclusion (inclusion thickness = 0.32 inch), the jog distance is larger than that for the thin inclusion (inclusion thickness = 0.1 inch).

(a)

Figure 4.8: Continued next page.

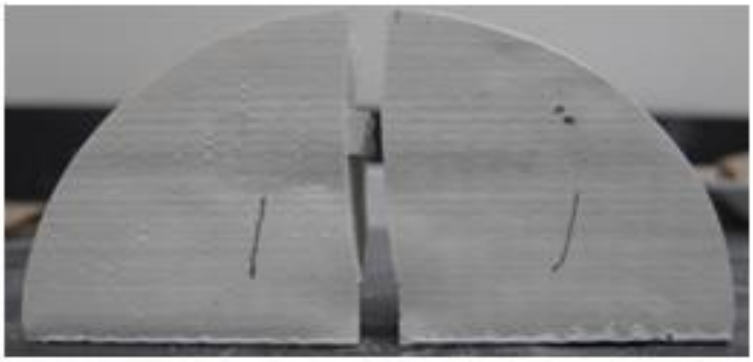

(b)

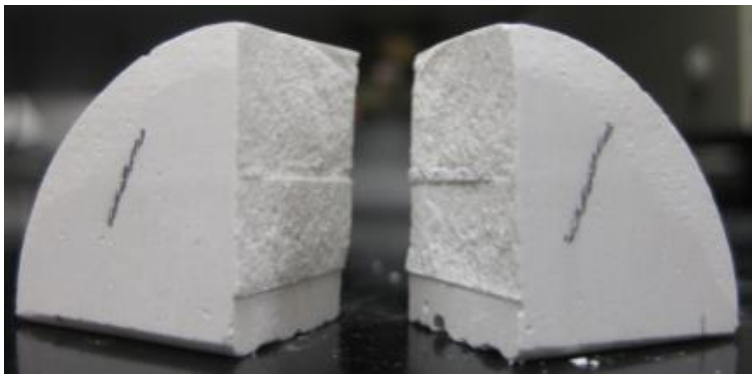

(c)

Figure 4.8: Hydrostone with plaster inclusion with different thickness (a) 0.32 in; (b) 0.2 in; (c) 0.05 in.

Another explanation for jog is due to the initiation of flaw on the upper interface. According to Zhang and Jeffrey's (2006) paper, for a hydraulic fracture propagating orthogonally to weak pre-existing natural fracture, if there is flaw located along the interface between rock and natural fracture, a new fracture may be initiated from the site of the flaw.

Maximum principal (most tensile) stress contour plots (Figure 4.9) show that as the crack starts propagating and approaches the inclusion, there will be a high tensile stress

region above the inclusion. The high tensile stress region occurs for both the thin inclusion sample (Figure 4.9) and thick inclusion sample (Figure 4.10), and could be the reason for jog.

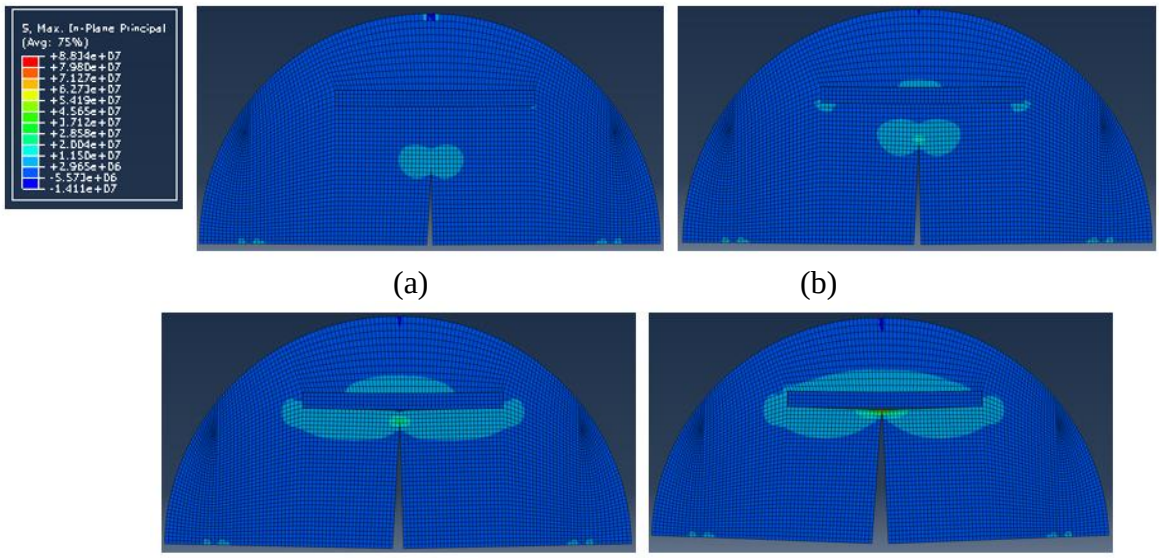

Figure 4.9: Maximum principal stress (most tensile) contour plots for thin inclusion sample.

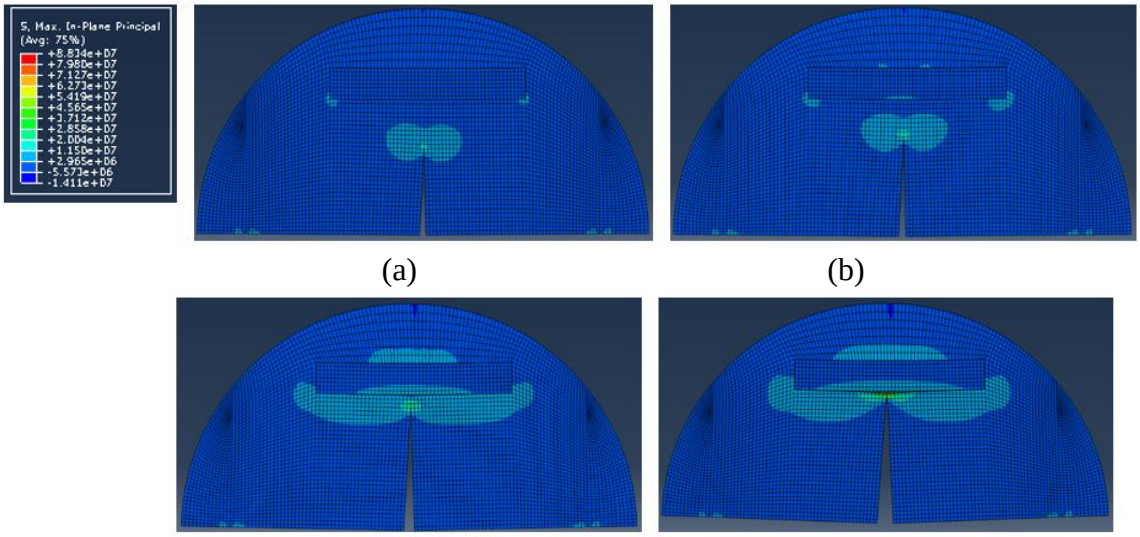

Figure 4.10: Maximum principal stress (most tensile) contour plots for thick inclusion sample.

4.4 SCB test on rock samples

Fracture propagation is strongly influenced by pre-existing inclusions. Both the approach angle and inclusion thickness will influence the crossing/diverting result. The SCB tests described so far were performed only on synthetic hydrostone samples. To work with a more realistic interfacial bonding between rock matrix and fracture cement fill, SCB tests were performed on mudstone rock sample of the Monterey Formation from southern California. While it is unfortunate that we have no geological context for these samples, they nevertheless have very interesting cemented fractures. The rock was first cut into slices with 0.5 in thickness. Natural fractures' crossing and jogging were observed in the rock slices (Figure 4.11).

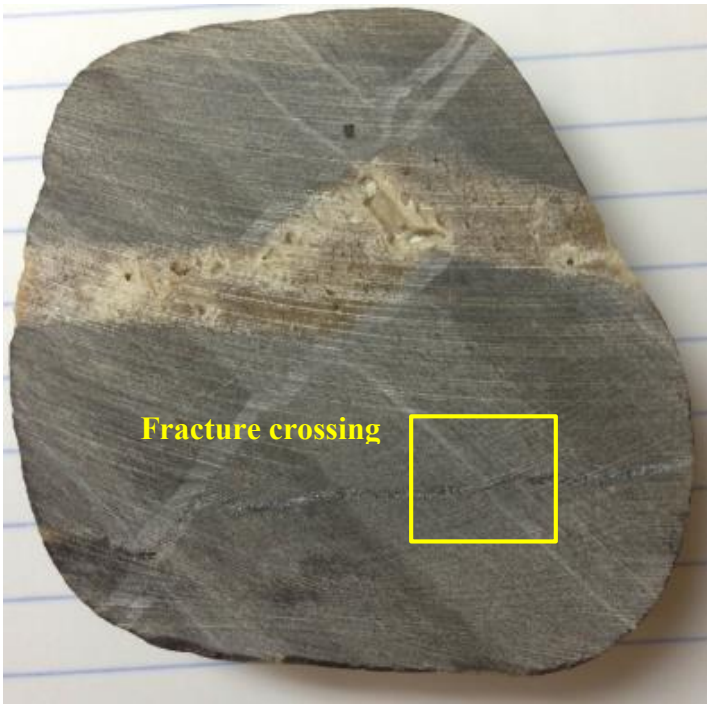

(a)

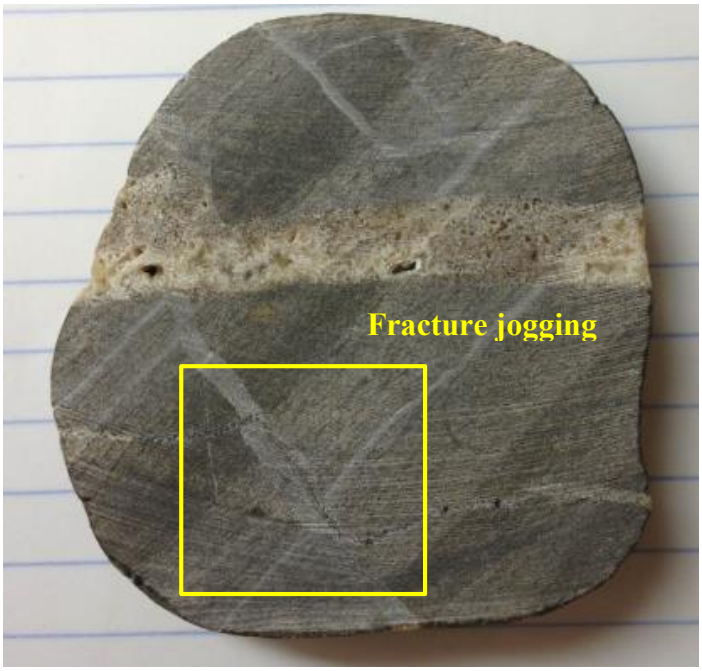

(b)

Figure 4.11: Mudstone slices showing natural fractures' crossing (a) and jogging (b).

SCB test samples were prepared using these mudstone slices (Figure 4.11). In order to minimize any damage to the cemented natural fracture during sample preparation, a low speed water saw was used for cutting. The final step was to use the grinding machine to smooth the sample edges in order to make semi-circular samples. Figure 4.12 shows the sample preparation procedure.

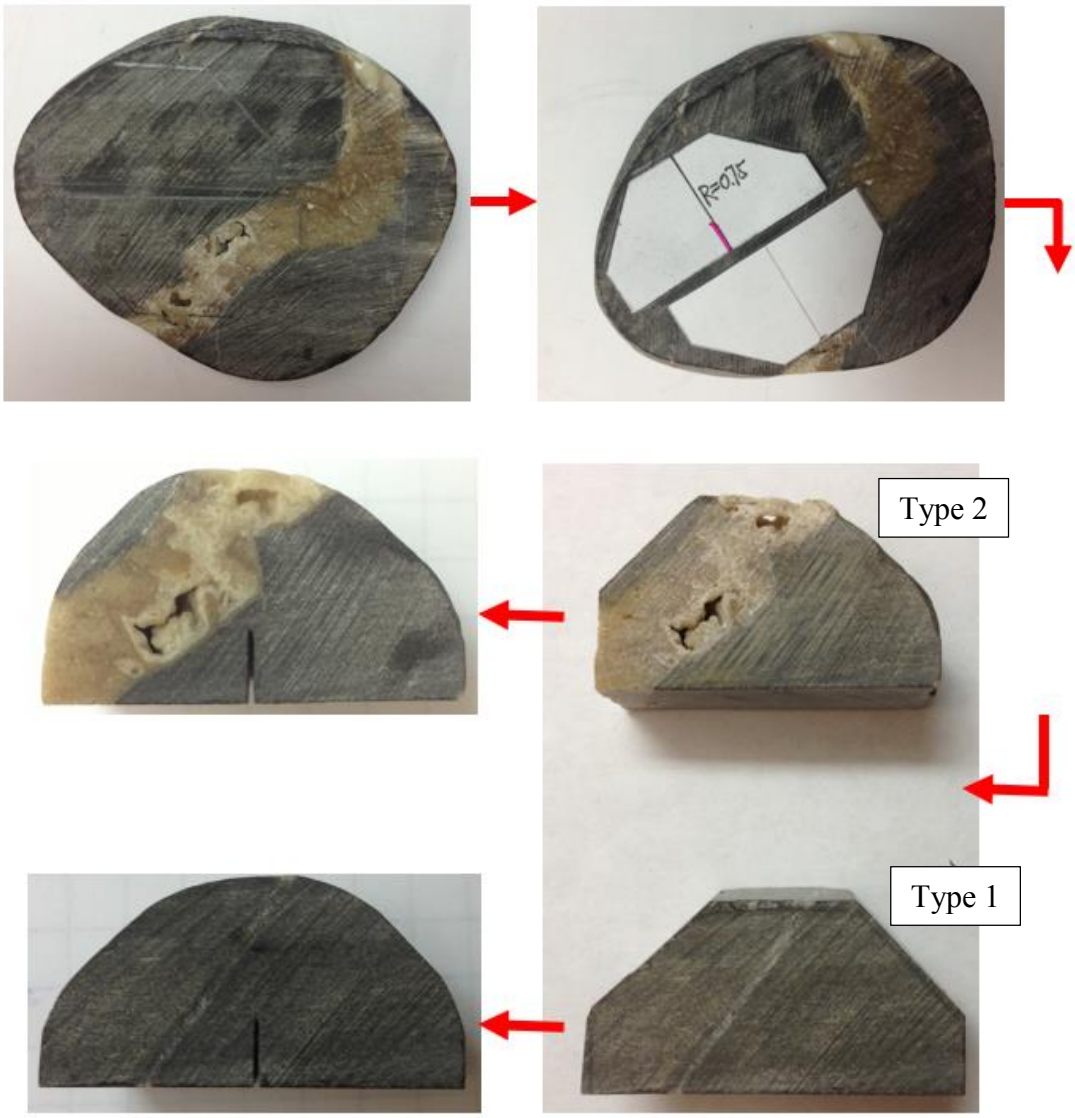

Figure 4.12: Mudstone sample preparation.

Two types of mudstone samples were prepared for SCB test. Type 1 (Figure 4.13) had a sample diameter of 1.5 in and a sample thickness of 0.5 in. The thickness of the naturally cemented fracture was about 0.06 in. We observed fracture crossing for a 90º approach angle and diversion for a 30º approaching angle, which was consistent with the previous hydrostone test results. However, instead of opening the interface between the rock and the natural fracture for crack path diversion as we saw in our synthetic hydrostone samples, the natural samples fractured within the cement.

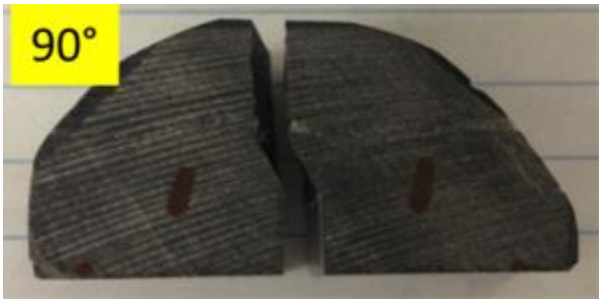

(a)

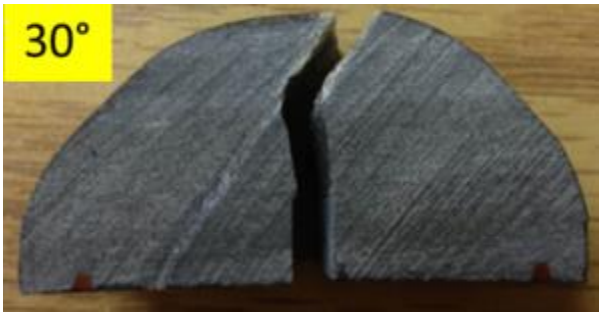

(b)

Figure 4.13: Continued next page.

(c)

Figure 4.13: Mudstone samples with different approach angles after SCB tests. Note that crack propagates within fracture cements, and not along the rock/cement interface.

The type 2 samples had natural fractures with thicknesses between 0.375~0.5 in and an approach angle of 30˚ (Figure 4.14). We observed propagating fracture crosses the natural fracture in sample (a). Although we observed large pores (vugs) within the natural fracture, they did not divert the propagating fracture. In the previous hydrostone test, propagating fractures always diverted into the natural fracture for samples with 30˚ approach angle. The main reason for this different behavior may be due to the difference of natural fracture thickness and its size in comparison to the entire sample. In order to reduce the natural fracture thickness effect, larger samples were prepared. Sample (b) in Figure 4.14 had a diameter of 2.25 in and sample (c) had a diameter of 2.625 in. We observed the propagating fracture crossing the natural fracture for these two samples, but there was some apparent diversion of path. In sample (c) (Figure 4.14), there was a small crack next to the notch before running the SCB test, this small crack allowed the fracture to propagate along the crack instead of the notch.

(a) Sample diameter = 1.5 in.

(b) Sample diameter = 2.25 in.

(c) Sample diameter=2.625 in.

Figure 4.14: Mudstone samples with different diameter

4.5 The effect of improved bonding on fracture propagation

For the real mudstone rock samples, fractures opened in the middle of the natural fracture when diverted for approach angles of less than 90 degrees, while in the synthetic hydrostone samples, fractures broke along the interface between the hydrostone and the inclusion slice. The controlling weakness of the inclusion-matrix interface seemed to be inconsistent with the real rock samples, so we modified our sample preparation procedures to try to improve the interfacial bonds for the synthetic samples.

Sandstone slices (1x1.5x0.1inches and 1x1.5x0.15 inches) were used to represent the inclusions. They were ground with coarse sand paper or grooved on both sides with a saw to increase the contact area (Figure 4.15).

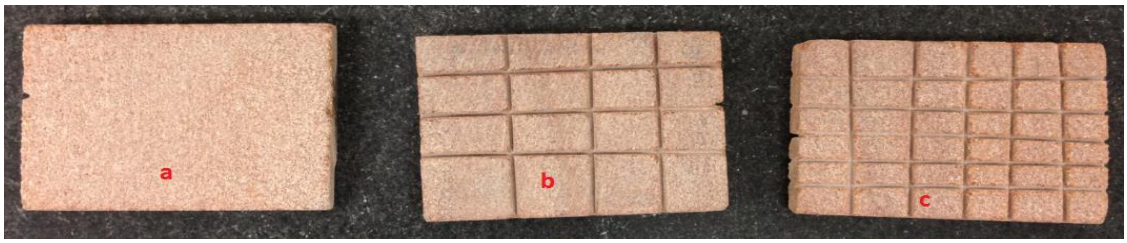

(a) (b) (c)

Figure 4.15: (a) Smooth inclusion slice prepared with sand paper; (b) Sparsely grooved inclusion, with three horizontal and three vertical grooves on both sides; (c) Densely grooved inclusion, with five horizontal and five vertical grooves on both sides.

Results showed that although the interface bonding strength was increased by creating grooves, the fracture diversion still happened on the interface. Another possible reason was because the grooves were placed from each side of the sample, so the inclusion was much thinner at the groove location. Sample 4 (Figure 4.16) had type c inclusion, the

fracture propagated along the inclusion after breaking it. The breakage happened on the interface between the hydrostone and the inclusion.

(a) (b)

Figure 4.16: Hydrostone with sandstone inclusion. The inclusion had 5 vertical and 5 horizontal grooves.

Besides the horizontal inclusion slices, we also tested vertical inclusion slices. The inclusion was placed on the same vertical plane as the initial crack. Test results also showed the separation at the interface between the inclusion and the hydrostone as the fracture propagating (Figure 4.17).

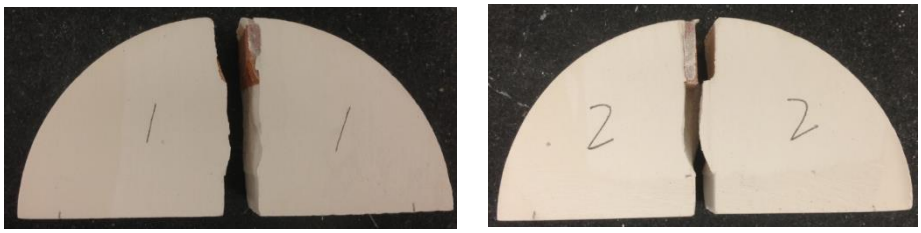

(a) (b)

Figure 4.17: Hydrostone with vertical sandstone inclusion.

The samples with grooves had higher effective toughness (K_I) than those without, and the greater the number of grooves, the greater the effective toughness. Samples in

Figure 4.19 had a 3 in diameter and a 0.1 in sandstone slice placed orthogonally to the initial vertical crack. Results showed that all samples had a propagating fracture that crossed the inclusion (Figure 4.18). Sample 1 had no grooves and the effective toughness (K_I) was 0.48 MPa$\sqrt{m}$. Sample 2 had three vertical and three horizontal grooves on each side of the inclusion, and K_{Ic} = 0.52 MPa$\sqrt{m}$. Sample 5 had 5 vertical and 5 horizontal grooves on each side, and the effective toughness was K_{Ic}=0.56 MPa$\sqrt{m}$.

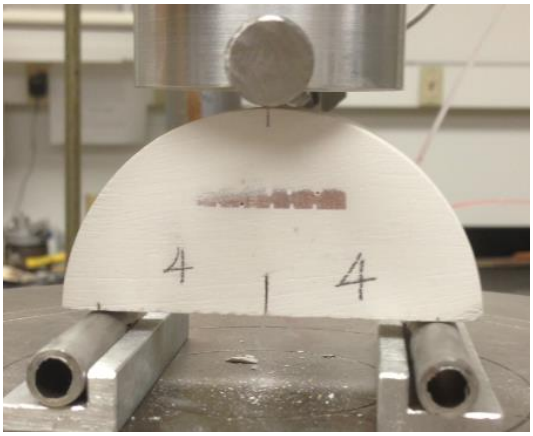

(a)

(b)

Figure 4.18: Continued next page.

(c)

Figure 4.18: Hydrostone with sandstone inclusion. Sample 1 had smooth inclusion, sample 2 had 3 x 3 grooves on each side of the inclusion, and sample 5 had 5 x 5 grooves on each side of the inclusion.

If the groove was not cemented very well when preparing the SCB sample, the empty space will lead to a very low effective toughness and the sample would break easily. Results showed that for the same 3-in diameter sample, if only about 50% of the grooves were cemented, the effective toughness decreased to 0.41~ 0.45 MPa$\sqrt{m}$.

Bonding is a very important parameter for SCB test and would cause the propagation path differ between the real rock sample and the synthetic rock sample. Although grooves increase bonding strength between the hydrostone and the sandstone inclusion, the propagating fracture is still opened along the interface. This implies that simple grooves on the inclusion cannot provide enough bonding strength on the hydrostone-inclusion interface. A better method should be developed in the future to provide a strong interfacial bonding for the sample.

CHAPTER 5: Conclusions and Future Work

In this report, semi-circular bending (SCB) tests were performed using synthetic hydrostone sample with inclusion. The inclusion slices with different strength, thickness and approach angles were used to mimic different types of cemented natural fractures. Samples with weaker inclusion were analogous to shale with calcite cement and samples with stronger inclusion were analogous to shale with quartz cement.

Lab results indicate that fracture propagation direction is strongly influenced by pre-existing inclusions. The propagating fractures are tend to cross inclusions with high approach angle and divert into inclusions with low approach angle. The crossing surface is not a clean cut, but with a jog distance depending on the inclusion thickness and approach angle. The inclusion thickness does not change the crossing/diverting result for orthogonal approaching samples, but it changes the jog distance along the interface. We also observe that, for sample with low approach angle inclusion, the initiated fracture curves toward the inclusion, which indicates the stress field is changed due to pre-existing inclusions.

The approach angle and inclusion thickness were also tested using mudstone rock with a more realistic interfacial bonding between rock matrix and fracture cement, and results are consistent are in good consistency. For the mudstone sample, results show that instead of opening the interface between the rock and the natural fracture as we see in synthetic samples, the natural samples are fractured within the cement. The bonding interface may play an important role in SCB test and would cause the propagation path different between the real rock sample and the synthetic rock sample. For future lab work,

a better bonding method should be generated to provide a stronger interface bond to be able to represent a more realistic behavior.

The implication of this experimental study is to provide insight into interactions between hydraulic and natural fractures for various interaction properties in real formation. Since natural fractures often occur in parallel sets, it is important to evaluate natural fracture orientation before hydraulic fracture treatments. Our results imply that if hydraulic fractures have lower approach angles, the ultimate fracture network is going to have higher complexity. The thickness of natural fractures can also add to the complexity (specifically, it can increase jogging distance). The overall result is the complex fracture network, which is in turn consistent with observations by micro-seismic measurements.

Subsurface reservoir rocks will normally be under compression from all directions and have some fluid pressure in the pores. These conditions will likely have an influence on fracture propagation, but are impossible to accommodate in standard SCB testing. Numerical model should be developed to address these shortcomings in the future.

References

Annual Energy Outluck 2013 early release reference case, EIA. From: http://www.eia.gov/pressro om/presentations/sieminski_12052012.pdf.

Anderson, R. G., Irons, B. M. and Zienkiewicz, O. C., 1968. Vibration and stability of plates using finite elements. International Journal of Solids and Structures, 4, 1033-55.

Anderson, T. L., 2004. Fracture mechanics: Fundamentals and applications.

Atkinson, B. K., 1989. Fracture Mechanics of Rock, 1st edition, Academic Press.

Bahorich, B. 2012. Examining the effect of cemented natural fractures on hydraulic fracture propagation in hydrostone block experiments. Master thesis.

Barton, M. and Rajan, S. D., 2000. Finite element primer for engineers. Available at: http://www.engr.mun.ca/~adfisher/7962-07/Presentations/FEA-Part1-HO.pdf.

Bayne, S. C., 2004. Chemistry of gypsum products. Available at: http://ute chdmd 2015.wikispaces.com/file/view/Dental%20material%20Gypsum-HO.pdf/172957631/De ntal%20material%20Gypsum-HO.pdf.

Blanton, T.L. 1982. An experimental study of interaction between hydraulically induced and pre-existing fractures. SPE/DOE 10847 Unconventional Gas Recovery Symposium, Pittsburgh, Pennsylvania, May 18-21.

Chong, K. P. and Kuruppu, M. D. 1984. New specimen for fracture toughness determination of rock and other materials. Int. J. Frac. 26: R59-R62.

Clark J. B., 1949. A hydraulic process for increasing the productivity of wells. AIME Trans., Vol. 186, 1-8.

Dahi-Taleghani, 2011. Analysis of hydraulic fracture propagation in fractured reservoirs: an improved model for the interaction between induced and natural fractures. PhD Thesis.

Dahi-Taleghani, A. and Olson, J. E. 2009. Numerical modeling of multi-stranded hydraulic fracture propagation: accounting for the interaction between induced and natural fractures. SPE 124884 SPE Annual Technical Conference and Exhibition, New Orleans, Louisiana, Oct. 4-7.

Daneshy, A., 2010. Hydraulic fracturing to improve production. The Way Ahead: Tech 101. 6(3), 14-17.

Fisher, N.K., Davidson, B.M., Goodwin, E.O., Buckler, W.S. and Steinberger, N. P. 2002. Integrating fracture mapping technologies to optimize stimulations in the Barnett Shale. SPE 77441 SPE Annual Technical Conference and Exhibition, San Antonio, Texas, Sept. 29-Oct.2.

Freund, L. B. and Suresh, S., 2003. Thin film materials: stress, defect formation and surface evolution.

Gale, J. F. W., Reed, R. M., and Holder, J., 2007. Natural fractures in the Barnett shale and their importance for hydraulic fracture treatments. AAPG Bulletin, V.91, 603-622.

Garg, A., Zwahlen, E., and Patzek, T. W., 1996. Experimental and numerical studies of one-dimensional imbibition in Berea sandstone. 16th Annual American Geophysical Union Hydrology Days, Fort Colllins, CO, Apr. 15-18.

Gu, H., Weng, X., Lund, J., Mack, M., Ganguly, U. and Suarez-Rivera, R. 2011. Hydraulic fracture crossing natural fracture at non-orthogonal angles: A criterion, its validation and applications. SPE 139984, SPE Hydraulic Fracturing Conference and Exhibition, The Woodlands, Texas, January 24-26.

Haberfriield, C. M. and Johnston, I. W., 1994. A mechanistically based model for rough rock joints. 0148-9062(93)E0024-I. Int. J. Rock Mech. Min. Sci. & Geomech. Abstr. Vol. 31, No. 4, 279-292.

Harlow, F. H. and Pracht, W. E., 1972. A Theoretical study of geothermal energy extraction. Journal of Geophysical Research, Vol. 27, No. 35.

Hubbert, M. K. and Willis, D. G., 1957. Mechanics of hydraulic fracturing. AIME Petroleum Transactions, 210, 153-163.

Le Calvez, J. H., Klem, R., Tanner, K.V., Bennett, L. and Craven, M., 2007. Real-time microseismic monitoring of hydraulic fracture treatment: a tool to improve completion and reservoir management. SPE 106159, SPE Hydraulic Fracturing Technology Conference, College Station, Texas, Jan.29-31.

Leonenko, Y. and Ghaderi, S., 2009. Reservoir modeling of Wabamun area CO2 sequestration project (WASP). Energy and Environmental Systems Group Institute for Sustainable Energy, Environment and Economy (ISEE), University of Calgary, Calgary, AB, Canada.

Lim I. L., Johnston, I. W. and Choi, S. K., 1994. Assessment of mixed-mode fracture toughness testing methods for rocks. Int. J. Rock Mech. & Min. Sci. & Geomech. Abstr. 31: 265-272.

Maxwell, S. C., Urbancic, T. I., Steinsberger, N. P., and Zinno, R., 2002. Microseismic imaging of hydraulic fracture complexity in the Barnett Shale, SPE 77440 SPE Annual Technical Conference and Exhibition, San Antonio, Texas, Sept. 29- Oct. 2.

Meng, C. and Pater, C. J., 2011. Acoustic monitoring hydraulic fracture propagation in pre-fractured natural rocks. Key Engineering Materials: Advances in Fracture and Damage Mechanics (514).

Nuismer, R. J., 1975. An energy release rate criterion for mixed mode fracture. International Journal of Fracture, Vol. 11, No. 2.

Olson, J. E., Bahorich, B. and Holder, J., 2012. Examining hydraulic fracture- natural fracture interaction in hydrostone block experiments, SPE 152618 SPE Hydraulic Fracturing Technology Conference, The Woodlands, Texas, USA, Feb. 6-8.

Park, N., Holder, J. and Olson, J. E., 2004. Discrete element modeling of fracture toughness tests in weakly cemented sandstone, ARMA/NARMS 04-553, the 6th North Americal Rock Mechanics Symposium: Rock Mechanics Across Borders and Disciplines, Houstone, Texas, Jun. 5-9.

Raziperchikolaee, S., Alvarado, V. and Yin, S., 2012. Effect of hydraulic fracturing on long-term storage of CO_2 in stimulated saline aquifers. Applied Energy, Vol. 102, Issue C, 1091-1104.

Renard, F., Bernard, D. Desrues, J. and Ougier-Simonin, A, 2009. 3D imaging of fracture propagation using synchrotron X-ray microtomography. Earth and Planetary Science Letters 286, 285-291.

Renshaw, C. E. and Pollard, D. D., 1995. An experimentally verified criterion for propagation across unbounded frictional interfaces in brittle linear elastic materials, Int. J. Rock Mech & Geomech. Abs., 32 237-241.

Rice, J. R., 1968. A path independent integral and the approximate analysis of strain concentration by notches and cracks. J. Appl. Mech. 35, 379-386.

Robinson, E. S., Rowley, J. C., Potter, R. M., Armstrong, D. E., McLnteer, B. B. and Mills, R. L. 1971. A preliminary study of the Nuclear subterrene. Los Alamos Scientific Laboratory, LA-4547.

Teufel, L. W. and Warpinski, N. R., 1983. Determination of in-situ stress from anelastic strain-recovery measurements of oriented core: applications to hydraulic fracture treatment design. SPE symposium on low permeability, Denver, CO, USA, Mar 14.

Thiercelin M. and Roegiers, J. C., 1986. Toughness determination with the modified ring test. Proc, 27th U.S. Symp. On Rock Mechanics, 615-622.

US DOE, 2009. Modern shale gas development 2009. http://yosemite.epa.gov/sab%5CSABPRODUCT.NSF/98C1AE492F70249C852576EF004A35D6/$File/Bkgrd+Doc-+Modern+Shale+Gas+Dev+in+the+US-A+Primer.pdf.

Valko, P. and Economides, M. J., 1995. Hydraulic fracture mechanics.

Wang, W., Olson, J. E. and Prodanovic, M., 2013. Natural and Hydraulic Fracture Interaction Study Based on Semi-Circular Bending Experiments. Unconventional Resources Technology Conference (URTeC), Denver, Colorado, Aug. 12-14.

Whittaker, B. N., Singh, R. N. and Sun, G., 1992. Rock fracture mechanics: principles, design, and applications, Elsevier.

Zhang, X. and Jeffrey, R. G., 2006. The role of friction and secondary flaws on deflection and re-initiation of hydraulic fractures at orthogonal pre-existing fractures. Geophys. J. Int. 166, 1454-1465.